Research Article

A Population of Innate Myelolymphoblastoid Effector Cell Expanded by Inactivation of mTOR Complex 1 in Mice

Fei Tang[1], Peng Zhang[1,2], Peiying Ye[1], Christopher A. Lazarski[1], Qi Wu[4], Ingrid L. Bergin[5], Timothy P. Bender[6], Michael N. Hall[7], Ya Cui[2], Liguo Zhang[3], Taijiao Jiang[2], Yang Liu[1,*] & Pan Zheng[1,*]

[1]Center for Cancer and Immunology Research, Children's Research Institute, Children's National Medical Center, Washington, DC 20010, USA

[2]Key Laboratory of Protein and Peptide Pharmaceuticals, [3]Key Laboratory of Infection and Immunity, Institute of Biophysics, Chinese Academy of Sciences, Beijing 100101, China

[4]Department of Neurology, [5]ULAM In-Vivo Animal Core, University of Michigan Medical School, Ann Arbor, MI 48109, USA

[6]Department of Microbiology, Immunology and Cancer Biology, University of Virginia, Charlottesville, VA 22908, USA

[7]Biozentrum, University of Basel, Klingelbergstrasse 50/70, CH-4056 Basel, Switzerland

Correspondence should be addressed to Pan Zheng (PZheng@cnmc.org) or Yang Liu (YaLiu@cnmc.org);

Abstract

Adaptive autoimmunity is restrained by controlling population sizes and pathogenicity of harmful clones, while innate destruction is controlled at effector phase. We report here that deletion of *Rptor* in mouse hematopoietic stem/progenitor cells causes self-destructive innate immunity by massively increasing the population of previously uncharacterized innate myelolymphoblastoid effector cells (IMLECs). Mouse IMLECs are $CD3^-B220^-NK1.1^-Ter119^-CD11c^{low/-}CD115^-F4/80^{low/-}Gr\text{-}1^-CD11b^+$, but surprisingly express high levels of PD-L1. Although they morphologically resemble lymphocytes and actively produce transcripts from Immunoglobulin loci, IMLECs have non-rearranged *Ig* loci, are phenotypically distinguishable from all known lymphocytes, and have a gene signature that bridges lymphoid and myeloid leukocytes. *Rptor* deletion unleashes differentiation of IMLECs from common myeloid progenitor cells by reducing expression of *Myb*. Importantly, IMLECs broadly overexpress pattern-recognition receptors and their expansion causes systemic inflammation in response to Toll-like receptor ligands in mice. Our data unveil a novel leukocyte population and an unrecognized role of Raptor/mTORC1 in innate immune tolerance.

Introduction

Autoreactive T and B lymphocytes are controlled by regulation of population sizes and pathogenicity through clonal deletion [1], clonal anergy [2] and regulatory T cells [3]. Through broadly-reactive pattern recognition receptors (PRRs) [4-5], innate immunity protects host against infections by both direct effector function and, indirectly, by induction of adaptive immunity [6-9]. Since innate immune responses triggered by host components can also cause fatal tissue damage[10-11], it must be properly regulated to protect hosts against self-destruction. Although a number of mechanisms have been proposed to prevent self-destructive innate effector functions [12-16], it is less clear if population sizes of innate effectors are suppressed to limit self-destruction.

The significance of protective self-tolerance mechanisms in adaptive immunity are revealed only when they have gone awry. For example, the significance of clonal deletion was elucidated when it was prevented by blocking either costimulation or antigen-expression in the thymus [17-18], while mice with Foxp3 mutation informed us of the consequence of defective regulatory T cells [19-20]. Since removal of the forbidden autoreactive T and B cells are achieved during T and B cell development [21-23], it is intriguing whether certain parallel mechanisms in innate immunity might also remain to be uncovered through genetic inactivation of key regulators in development of innate effector cells.

The hematopoietic system is among the best characterized of all tissue/systems in mammalians, with cell types and lineages clearly defined in the context of developmental stages and localization [24-25]. Hematopoiesis in bone marrow (BM) is responsible for generation of major lineages of innate effectors, including NK cells, granulocytes, monocytes and dendritic cells. While genetic switch in generation of innate immune system has been identified [25], we are not aware of defects that predispose host to innate immune attack through increasing population sizes of self-destructive innate effectors.

The mammalian target of rapamycin (mTOR) pathway, which couples energy and nutrient abundance to the execution of cell growth and division, has emerged as a major regulator of hematopoiesis. Thus, activation of mTOR complex 1 (mTORC1) by deleting *Tsc1*, which encodes a negative regulator for mTORC1 [26], causes loss of hematopoietic stem cell (HSC) function and renders mice prone to leukemiogenesis in conjunction with loss of tumor suppressor *Pten*[27-29]. More recently, two groups reported that deletion of *Rptor*, which encodes a critical component of mTORC1 [30-31], dramatically perturbed hematopoiesis in mice [32-33], as evidenced by defects in production of mature lymphoid and myeloid cells. Remarkably, cells with $CD11b^{+}$ $Gr\text{-}1^{-}$ surface markers massively accumulated in BM following *Rptor* deletion in HSCs [32-33]. The nature of this population and consequences of their accumulation, however, remains a mystery.

Here we systematically analyzed the gene expression signature, cell surface markers, morphology and functions of the $CD11b^{+}Gr\text{-}1^{-}$ population in the *Rptor*-deficient BM and other organs and sought for their physiological counterpart in the normal mice. We found that these cells can be identified in both normal and *Rptor*-deficient hosts by $CD3^{-}B220^{-}NK1.1^{-}Ter119^{-}$ $CD11c^{low/-}CD115^{-}F4/80^{low/-}Gr\text{-}1^{-}$ $CD11b^{+}PD\text{-}L1^{+}$ markers, lymphoid morphology and actively transcribed *Ig* loci. Interestingly, these cells broadly express essentially all TLRs along with many other pattern recognition receptors and mounted a greatly exacerbated response to all TLR ligands tested. We name this population IMLEC for innate myelolymphoblastoid effector cell that can be derived from common myeloid progenitors. Because their expansion and broad distribution render the host vulnerable to TLR ligands, we suggest that mTORC1-mediated repression of IMLEC expansion represents a new mechanism of immune tolerance in the innate immunity. Our study also raises an intriguing perspective that while repressing mTOR over-activation suppresses leukemia, a functional mTORC1 must be maintained to limit generation of IMLECs to avoid innate immune destruction.

Results

Raptor suppresses accumulation of a previously uncharacterized subset of leukocytes with features of both myeloid and lymphoid cells

As germline deletion of *Rptor* (which encode the Raptor protein) is embryonic-lethal, we crossed mice harboring homozygous loxp-flanked *Rptor* exon 6 [34] to those with interferon-inducible *Mx1-Cre* recombinase transgene, which allows inducible deletion of target genes effectively in the hematopoietic system upon treatment of interferon or its inducers [35]. We treated the 6-8 weeks old *Rptor* $^{F/F}$ and *Rptor* $^{F/F}$,*Mx1-Cre* mice with polyinosinic: polycytidylic acid (pIpC) every other day for 2 weeks to induce the deletion of *Rptor*. Hereafter, we refer to the pIpC-treated *Rptor* $^{F/F}$ mice as Ctrl (control) mice, while the *Rptor* $^{F/F}$*, Mx1-Cre* mice as cKO (conditional knockout) mice (***Figure 1A*** and ***Figure 1—figure supplement 1***). As has been reported by others [32-33], *Rptor* deletion causes broad defects in all lineages of hematopoietic cells (see also ***Figure 1—figure supplement 1, 2, 3***). However, the number of hematopoietic stem/progenitor cells (HSPCs) increased (***Figure 1—figure supplement 4***). Most notably, $CD11b^+$ $Gr\text{-}1^-$ cells, which amount to nearly 50% of BM cells in our model, emerge at the expense of $CD11b^+$ $Gr\text{-}1^+$ granulocytes from the cKO mice (***Figure 1B, C***). Importantly, we also observed the massive accumulation of $CD11b^+Gr\text{-}1^-$ cells in the BM of *Rptor*$^{F/F}$, *Cre-ER* mice after tamoxifen induced targeted mutation of *Rptor*, which clearly excludes the role of pIpC in the generation of these cells (***Figure 1—figure supplement 5***).

The $CD11b^+$ $Gr\text{-}1^-$ cells were smaller and had reduced granularity when compared to $CD11b^+$ $Gr\text{-}1^+$ granulocytes, but were larger and more granular than the $CD11b^-$ $Gr\text{-}1^-$ cells (***Figure 1—figure supplement 2E, F***). Surprisingly,

despite the expression of myeloid marker CD11b on the expanded population of BM cells, histological analysis of BM section revealed pervasive expansion of lymphoblastoid cells (***Figure 1D***). The cKO BM contained markedly decreased erythroid and myeloid lineage cells and markedly increased lymphocytes. Lymphocytes were predominantly small-to-medium sized and had normal cytological features. There was also an increased population of large blast-like cells with prominent nucleoli and perinuclear clearing resembling lymphoblasts. Plasma cells were present in small numbers. The myeloid: erythroid ratio was within normal range (3.04) but the overall number of erythroid and myeloid cells was very low. In particular, very few erythroid cells were present. In the myeloid lineage there was also maturation disruption since immature ring form neutrophils (neutrophilic metamyelocytes) predominate over mature neutrophils (condensed chromatin) (***Figure 1D***). Giemsa staining of BM smear revealed a massively increased lymphoblast population and severe depletion of both immature erythroid cells and granulocytes in the cKO mice (***Figure 1E***). These cells were replaced by cells with prominent nucleoli and perinuclear clearing resembling lymphoblasts. To confirm that the lymphoblasts were the $CD11b^{+}$ $Gr\text{-}1^{-}$ cells identified by flow cytometry in the cKO BM (***Figure 1B, C***), we FACS-sorted the subset based on $CD11b^{+}$ $Gr\text{-}1^{-}$ surface markers and validated its lymphoid morphology (***Figure 1F***).

The spleen was greatly enlarged due to expansion of the follicular centers and periarteriolar sheaths within the splenic white pulp (lymphoid areas) of the cKO

mice (***Figure 1—figure supplement 1C***). The expanding white pulp populations consisted of lightly stained, large cells that morphologically resembled germinal center lymphocytes. In some areas, these populations expanded within the marginal zones while in others, they involved the periarteriolar sheaths. The cells had an increased amount of pale eosinophilic cytoplasm and mild pleomorphism with both centroblast-like cells (larger cells with large ovoid nuclei and 1-2 prominent nucleoli per cell) and centrocyte-like cells (smaller cells with cleaved or elongated nuclei and unapparent nucleoli)..

Since cells with such combination of morphology and surface markers had not been identified previously, we FACS-sorted the $CD11b^{+}$ $Gr\text{-}1^{-}$ cells from the *Rptor* cKO BM and carried out next-generation RNA sequencing (RNA-seq). Using principal component analysis (PCA), we compared gene expression profiles of these $CD11b^{+}$ $Gr\text{-}1^{-}$ cKO BM cells with other known subsets of hematopoietic cells, including B cells, T cell subsets, NK cells, myeloid cell subsets, dendritic cells and erythroid cells. This analysis demonstrates that the $CD11b^{+}Gr\text{-}1^{-}$ cKO BM cells were distinct from all known blood cell types, although they appear to be closely related to B lymphocytes and macrophages (***Figure 1G***). We hereafter refer these cells as innate myeloidlymphoblastoid effector cells (IMLECs).

We identified subset specific genes using a threshold of 4-fold changes and an adjusted FDR-adjusted p-value <0.01. As shown in ***Figure 2A***, by comparing RNA-seq data-based gene expression signature of all known leukocyte subsets,

a unique gene expression signature was identified in the CD11b^{+} Gr-1^{-} cKO BM IMLECs. The signature consists of 48 genes that are up-regulated by more than 4-fold. The 48 genes over expressed in the CD11b^{+} Gr-1^{-} cKO BM IMLECs are listed in ***Figure 2B***. Among their diverse functions, these genes are involved in intracellular signaling cascades (such as *Arhgap31*, *Rab20*, *Gna12*, *Mink1* and *Prkch*) and metabolic processes (such as *Naga*, *Atf3*, *Aoah*, *Chst14* and *Gns*). The uniqueness of cKO BM IMLEC is also supported by pair-wise comparisons between IMLEC and peritoneal macrophage or other closely related cell types that are prominent in BM (***Figure 2—figure supplement 1***).

A defining feature of the B cell lineage is activation of *Ig* gene loci, as evidenced by "sterile" transcripts transcribed from the unarranged loci of Ig heavy chain (*Igh*) and light chains *(Igk* and *Igl*) [36]. RNA-seq data revealed high levels of sterile transcripts within the *Igh* locus (***Figure 2C***) and *Igk* and *Igl* loci (***Figure 2—figure supplement 2***) from both B cell lineages and cKO BM IMLECs. This is a significant difference from macrophage, which had no detectable expression of the sterile transcripts, as expected. Another defining feature of developing B-lymphocytes is *Ig* gene rearrangement, a unique mechanism of genetic recombination that occurs only during the early stages of B cell maturation. This process is strictly dependent on recombinases genes *Rag1* [37-38] and *Rag2* [39-40]. As shown in ***Figure 2D***, no expression of *Rag1* was detectable by quantitative PCR (qPCR), although a detectable but extremely low level of *Rag2* was observed. Consistent with lack of *Rag1* expression, no gene rearrangement was

found in the *Ig* loci (***Figure 2E***). Taken together, our data so far demonstrate that Raptor suppresses accumulation of a previously uncharacterized leukocyte subset with features of both myeloid and lymphoid cells.

Characterization of IMLECs in *Rptor* cKO and WT mice

IMLECs identified in the *Rptor* cKO mice did not express surface markers that are used to define other lymphocytes, such as B220 for B cells, CD3 for T cells and NK1.1 for NK cells (***Figure 3A***). The high levels of CD11b indicated that these cells are distinct from the recently identified innate lymphoid cells (ILCs) that are CD11b negative [41]. In addition, they lack surface markers for progenitor cells, such as c-Kit and Sca-1 (***Figure 3A***). Although the cKO IMLECs retained a high level of myeloid marker CD11b, they expressed a very low level of F4/80 macrophage marker and lacked CD115 monocyte marker (***Figure 3B***). To identify a positive marker for IMLEC, we searched our RNA-seq database for overexpression of genes that encode cell surface CD (cluster of differentiation) markers. Among 317 CD markers (***Supplementary file 1***), the most up-regulated gene in the cKO BM IMLECs over Ctrl whole BM cells was *Cd274* (also called *B7h1* or *Pdl1*). As shown in ***Figure 3B*** and ***Figure 3C***, PD-L1 was expressed on the vast majority of $CD11b^{+}$ $Gr\text{-}1^{-}$ BM cells from *Rptor* cKO mice.

Based on the above data and availability of robust cell surface markers, we define IMLECs by their expression of CD11b and PD-L1, but lack of major lineage markers for T cells (CD3), B cells (B220), natural killer cells (NK1.1),

erythroid cells (Ter119), granulocytes (Gr-1), macrophages and monocytes (F4/80 and CD115). These markers allowed us to search wild-type BM for IMLEC. Interestingly, a clear although small fraction of the Lin^- ($CD3^-B220^-$ $NK1.1^-$ $Ter119^-$ $Gr\text{-}1^-$ $F4/80^-$ $CD115^-$) $CD11b^+$ BM cells in the Ctrl mice also expressed PD-L1 (***Figure 3C***, left panel), although the overall PD-L1 expression level was not as high as that from cKO IMLECs. Following *Rptor* deletion, a robust expansion (approximately 500-fold) of Lin^- $CD11b^+$ $PD\text{-}L1^+$ BM IMLECs was observed (***Figure 3C***, right panel).

It should be noted that although cKO IMLECs also over-express *Cd11c* gene (***Supplementary file 1***), IMLEC gene expression profiles are distinct from dendritic cell (DC) based on gene signature (***Figure 1G*** and ***Figure 2—figure supplement 1E, F***). In cKO IMLECs, the CD11c levels were somewhat lower than the $PD\text{-}L1^-$ DC (***Figure 3D***). In WT mice, greater than 90% of Lin^- $CD11b^+PD\text{-}L1^+$ IMLEC in BM, lung and peripheral blood mononuclear cells expressed only low levels of CD11c, while those in spleen and mesenteric lymph nodes consisted of two major subsets: $CD11c^{high}$ and $CD11c^{low/-}$ (***Figure 3E***). IMLECs were also found among the leukocytes isolated from lung and in peripheral lymphoid organ (***Figure 3F, 3G, 3H***), and this population was greatly expanded in the cKO mice (***Figure 3I***).

To further confirm that this subset is the IMLEC in normal BM, we FACS-sorted the Lin^- ($CD3^-$ $B220^-$ $NK1.1^-$ $Ter119^-$ $Gr\text{-}1^-$ $F4/80^-$ $CD115^-$) $CD11b^+$ $PD\text{-}L1^+$ cells

from wild type (WT) BM and characterized their morphology and levels of sterile *Ig* transcripts. As shown in ***Figure 4A***, the sorted cells had a lymphoid morphology as did the cKO IMLECs. They also displayed comparable size and granularity as cKO IMLECs (***Figure 4B***). Moreover, $Lin^-CD11b^+PD\text{-}L1^+$ cells from WT BM expressed sterile transcripts of *Ig* loci identified by RNA-seq (***Figure 4C***). Furthermore, subsequent validation of IMLECs in WT BM was undertaken by comparing the expression of other top candidate markers (CD14, CD16) and MHC-I/MHC-II (***Figure 4—figure supplement 1A***), as well as population-specific transcription factors *Mitf*, *Atf3* and *Zdhhc1* (***Figure 4 D, E***). The largely comparable expression levels of these surface markers and transcription factors between WT and cKO IMLECs provide additional lines of evidence for these cells to be naturally occurring IMLECs. Therefore, a small fraction of normal leukocytes in lymphoid and non-lymphoid tissues have the IMLEC phenotype, and this subset is massively expanded after *Rptor* deletion.

Altered differentiation is responsible for accumulation of IMLECs

Theoretically, expansion of IMLECs in cKO BM may be caused by increased proliferation and/or reduced apoptosis. To test this possibility, we analyzed the proliferation of IMLECs by Ki-67 staining and BrdU incorporation. Remarkably, $Lin^-CD11b^+PD\text{-}L1^+$ IMLECs from both Raptor Ctrl and cKO BM had much fewer $Ki\text{-}67^+$ cells (***Figure 4F,G***) or $BrdU^+$ cells (***Figure 4—figure supplement 1B, C***) when compared with other lineages. The fact that IMLECs are not proliferating at

a higher rate than other BM cell types effectively rules out rapid proliferation as an explanation for IMLECs accumulation in Raptor cKO BM. Likewise, the massive increase of IMLEC in cKO mice over those in the Ctrl mice cannot be due to proliferation, as the percentage of Ki-67$^+$ or BrdU$^+$ cells is not increased in cKO mice. Furthermore, based on cell surface Annexin V staining, IMLECs from cKO BM were more prone to apoptosis than total lineage$^+$ population (***Figure 4H, I***) and had apoptosis rate that was comparable to granulocytes, B cells and T cells in BM (***Figure 4—figure supplement 1D, E***). The pronounced apoptosis also rules out the possibility that increased survival may account for preferential accumulation of IMLECs in cKO mice. The robust apoptosis detected among WT IMLECs likely contributed to the reduced amount of IMLECs in normal BM (***Figure 3C***). Consistent with the reduced proliferation and increased apoptosis of IMLECs, our exhaustive efforts to demonstrate self-renewal of IMLEC through transplantation of massive numbers of IMLEC have all been unsuccessful (data not shown).

As an alternative hypothesis, we evaluated whether IMLECs accumulated because of altered differentiation of hematopoietic stem and progenitors (HSPCs). As the first step to test this hypothesis, we evaluated if IMLEC accumulation in cKO BM was cell-intrinsic. Briefly, we mixed either *Rptor*$^{F/F}$ or *Rptor*$^{F/F}$*, Mx1-Cre* (both CD45.2$^+$) BM cells with recipient type CD45.1$^+$ WT BM cells at a 2:1 ratio. At six weeks after BM transplantation, *Rptor* was deleted from the *Rptor*$^{F/F}$*, Mx1-Cre* donor-derived cells by pIpC treatment (***Figure 5A***).

As shown in ***Figure 5B***, the accumulation of $CD11b^+$ $Gr\text{-}1^-$ IMLECs was intrinsic to *Rptor* $^{-/-}$ BM cells. Since our earlier data suggested that IMLECs accumulated at the expense of granulocytes (***Figure 1B, C***), we tested if granulocytes were converted to IMLECs following *Rptor* deletion. We produced *Rptor*$^{F/F}$*, Lyz2-Cre*$^{+/+}$ mice that should have myeloid lineage-specific deletion of *Rptor*. However, despite the effective deletion of the *Rptor* gene in the granulocytes (***Figure 5C***), the percentages of $CD11b^+$ $Gr\text{-}1^+$ granulocytes and $CD11b^+$ $Gr\text{-}1^-$ IMLECs were unchanged (***Figure 5D***). These data suggest that accumulation of IMLEC in the cKO mice was not due to trans-differentiation from granulocytes.

Next, we use both *in vitro* co-culture and *in vivo* BM transplantation to identify the progenitor that may give rise to IMLECs. We co-cultured OP9 stromal cells with FACS-sorted BM LSK (Lin^- $Sca\text{-}1^+$ $c\text{-}Kit^+$), CMP (Lin^- $Sca\text{-}1^-$ $c\text{-}Kit^+$ $CD34^{Medium}$ $CD16/32^{Medium}$) and CLP (Lin^-CD127^+ $Sca\text{-}1^{Medium}c\text{-}Kit^{Medium}$) populations from Ctrl and cKO mice that had been treated with pIpC (***Figure 5E***). As shown in ***Figure 5F***, both LSK and CMP populations from *Rptor*$^{-/-}$ BM gave rise to $CD11b^+$ $Gr\text{-}1^-$ $PD\text{-}L1^+$ IMLECs. As expected, *Rptor*-sufficient CLPs were not able to give rise to $CD11b^+$ myeloid cells. Interestingly, *Rptor*-deficient CLPs generated progenies with a small portion exhibiting immunophenotypes of IMLECs. We also transplanted sorted LSK and CMP populations and induced *Rptor* deletion in the donor cells by treating recipients with pIpC (***Figure 5G***) to confirm their ability in giving rise to IMLECs. Due to lack of self-renewal activity of progenitor cells and rapid apoptosis of IMLEC, we used a much shorter timeline than the whole bone

marrow transplantation studies in order to capture progenitor-derived IMLEC. As shown in ***Figure 5H***, deletion of *Rptor* in either LSKs or CMPs was sufficient to induce the generation of $CD11b^+$ $Gr\text{-}1^-PD\text{-}L1^+$ cells in recipients BM. The shorter timeline explained relative paucity of LSK-derived IMLEC when compared with long-term bone marrow transplantation (***Figure 5A, B***). As expected, since CMPs do not have self-renewal capability, only a small number of progeny cells were produced. However, since IMLEC can be generated from CLP *in vitro*, their potential to do so under physiological conditions cannot be ruled out. Taken together, our data demonstrate that the massive accumulation of IMLECs in cKO mice can be caused by altered differentiation of CMPs, although other differentiation pathway cannot be ruled out.

Reduced c-Myb expression is responsible for accumulation of IMLECs

A previous study demonstrated that heterozygous *Myb* mutation leads to an expansion of BM $CD11b^+Gr\text{-}1^-$ cells [42]. Although expression of PD-L1 was not evaluated in the earlier study, we were intrigued by the possibility that down-regulation of *Myb* may be the underlying mechanism for the massive production of IMLECs. Since both LSKs and CMPs are able to give rise to $CD11b^+$ $Gr\text{-}1^-$ $PD\text{-}L1^+$ IMLECs, we evaluated expression of c-Myb in both LSK and CMP populations. Indeed, the *Myb* transcripts were significantly reduced in both LSK and CMP populations sorted from *Rptor* cKO mice (***Figure 6A***). Moreover, our intracellular staining also revealed reduced levels of c-Myb protein in both LSKs and CMPs from cKO BM (***Figure 6B***). Interestingly, induced deletion of c-Myb in

mice with homozygous floxed c-Myb (*Myb*$^{F/F}$, *Mx1-Cre*), but not heterozygous floxed c-Myb (*Myb*$^{F/+}$, *Mx1-Cre*), showed obvious increase of PD-L1 expression in CD11b^{+}Gr-1^{-} BM cells (***Figure 6C, D, E*** and ***Figure 6—figure supplement 1A, B, C***), despite of significant decrease of BM whole leukocytes due to *Myb*-reduction induced cell apoptosis. To avoid excessive apoptosis and test if the down-regulation of *Myb* was necessary and sufficient to cause accumulation of IMLECs, we transplanted BM cells from either *Myb*$^{F/F}$, *Rag2*$^{-/-}$ or *Myb*$^{F/F}$, *Rag2*$^{-/-}$, *CreER* mice to CD45.1^{+} recipients, which then received tamoxifen to achieve deletion of *Myb* specifically in donor-derived hematopoietic cells after their full reconstitution (***Figure 6F***). Consistent with essential role for c-Myb in hematopoiesis, surviving leukocytes appeared heterozygous for *Myb* deletion (***Figure 6G***). As early as 1 week after the first injection of tamoxifen, a significant decrease in CD11b^{+} Gr-1^{+} granulocytes and an increase in CD11b^{+} Gr-1^{-} PD-L1^{+} IMLECs were observed in *Myb* cKO BM (***Figure 6H***). Moreover, the provision of heterologous c-Myb significantly diminished the generation of IMLECs from Raptor-deficient LSK cells in our *in vitro* OP9 co-culturing experiments (***Figure 6—figure supplement 1D, E, F, G***). Therefore, down-regulation of *Myb* is necessary for production of IMLECs.

We recently reported that deletion of *Rptor* caused up-regulation of miRNA biogenesis in HSPCs [43]. We searched our miRNA microarray database and mirSVR score database[44] for potential impact of miRNAs in down-regulation of *Myb* expression. Using the stringent criteria of mirSVR score <-1.0, we identified

50 miRNAs that presented in the HSPCs (***Supplementary file 2***). Among them, 13 miRNAs showed >2.0 folds up-regulation in the *Rptor*-deficient HSPCs (P<0.05), while none showed statistically significant down-regulation (***Figure 6I***). Significant up-regulation of miR-150 (1.4 folds increase, P=0.05), which was previously demonstrated to inhibit *Myb* expression [45-46], was also observed. Up-regulation of *Myb*-targeting miRNAs provides a plausible mechanism for down-regulation of *Myb* by *Rptor* deletion. However, the broad spectrum of the up-regulated miRNAs suggests that it is unlikely that a single miRNA is responsible for the overall reduction of *Myb* expression.

Expansion of IMLECs associated with lethal inflammatory response to TLR ligands

RNA-seq data indicated that IMLECs broadly up-regulate pattern recognition receptors (PRRs) genes. TLRs, the first family of PRRs identified, were broadly over-expressed in cKO IMLECs as determined by RNA-seq (***Figure 7A***). RT-PCR confirmed that IMLECs from both cKO and WT mice over-expressed essentially all TLRs tested, particularly *Tlr2*, *Tlr3*, *Tlr4*, *Tlr6*, *Tlr7*, *Tlr8* and *Tlr9* (***Figure 7B***). In addition to TLRs, expression of other PRRs, including NLRs, ALRs and RLRs, was also broadly elevated (***Figure 7—figure supplement 1***). When the BM from Ctrl and *Rptor*$^{-/-}$ mice were compared for their responses to TLRs agonists, including synthetic *tripalmitoylated lipopeptide* Pam3CysSerLys4 (Pam3CSK4, TLR1/2 agonist), heat-killed *Listeria monocytogenes* (HKLM, TLR2 agonist), synthetic analog of double-stranded RNA poly I:C (pIpC, TLR3 agonist),

lipopolysaccharide (LPS, TLR4 agonist), flagellin from *Salmonella typhimurium* (FLA-ST, TLR5 agonist), synthetic lipoprotein derived from *Mycoplasma salivarium* (FSL-1, TLR2/6 agonist), single-stranded RNA Double-Right complexed with LyoVec™ (ssRNA-DR, TLR7 agonist) and synthetic oligonucleotides containing unmethylated CpG dinucleotides (ODN1826, TLR9 agonist), it is clear that *Rptor*$^{-/-}$ BM increased production of TNF-α (***Figure 7C***) and MCP-1(***Figure 7D***) in response to all TLR ligands tested. To determine the cellular basis for the enhanced cytokine production, we used intracellular and cell surface staining to identify cells that produced the inflammatory cytokines. As shown in ***Figure 7E***, IMLECs from both WT and *Rptor* cKO BM were potent producers of TNF-α when stimulated by LPS.

Consistent with exacerbated responses to TLR ligands in BM cells, deletion of *Rptor* in cKO mice resulted in massive increase in inflammatory cytokines in serum (***Figure 8A***). Approximately 40% of cKO mice died within 2 months after 7 pIpC treatments (***Figure 8B***). Histological analyses revealed extensive inflammation in the liver with associated tissue injuries (***Figure 8C***). A substantial proportion of the leukocytes in the liver of cKO mice were IMLECs, as demonstrated by cell surface markers CD11b^{+} Gr-1^{-} PD-L1^{+} F4/80$^{low/-}$ (***Figure 8D, E***). To test if the mice with expanded IMLECs were more sensitive to endotoxin, we challenged the Ctrl and cKO mice with low doses of LPS (5mg/kg body weight). While all Ctrl mice survived the LPS challenge, all cKO mice succumbed within 36 hours (***Figure 8F***). The dramatically increased mortality due to

endotoxic shock was associated with remarkably elevated levels inflammatory cytokines. As shown in ***Figure 8G*** and ***Figure 8H***, a more than 500-fold increase in TNF-α and an approximately 10-fold increase of MCP-1 were detected in the serum of cKO mice at 6 hours after LPS injection. It has been demonstrated that acetaminophen-triggered liver necrosis induces HMGB-1-mediated inflammatory responses to danger-associated molecular patterns (DAMPs)[11, 47]. As shown in ***Figure 8I*** and ***Figure 8J***, cKO mice mounted a significantly elevated inflammation to challenge by low doses of acetaminophen. Therefore, amplification of IMLEC also leads to elevated response to tissue injuries.

Since *Mx1-Cre* was broadly activated after pIpC treatment, it is less certain whether the increased sensitivity of the cKO mice to TLR ligands is due to immunological abnormality. To address this issue, we produced chimeric mice in which pIpC induces deletion of the targeted gene exclusively in hematopoietic cells by transplanting *Rptor*$^{F/F}$*, Mx1-Cre* (CD45.2^{+}) BM cells into lethally irradiated CD45.1^{+} recipients. After hematopoietic reconstitution, the recipients were treated with 3 doses of pIpC to induce deletion of *Rptor* exclusively in the hematopoietic cells. After 10 days of pause, the Ctrl and cKO chimera mice were challenged with new pIpC injection and monitored for survival (***Figure 9A***). As shown in ***Figure 9B***, while a large portion of the cKO chimera mice died progressively starting within a week of the second round of pIpC treatment, all Ctrl chimera mice survived the observation period of more than 45 days.

Massive leukocytes infiltration was observed in the liver of cKO chimeric mice (***Figure 9C***). Cell surface phenotyping of the donor-type leukocytes in BM (***Figure 9D***), spleen (***Figure 9E***) and liver (***Figure 9F***) revealed accumulation of $CD11b^{+}$ $Gr\text{-}1^{-}$ $PD\text{-}L1^{+}$ $F4/80^{low/-}$ IMLECs. Collectively, the data in ***Figure 8*** and ***Figure 9*** demonstrate that over-expansion of IMLECs, as a result of *Rptor* deletion, renders the host highly vulnerable to TLR ligands.

Discussion

We have characterized a leukocyte population, which we called IMLECs, that has a strong innate effector function but with features of both myeloid and lymphoid cells. Furthermore, our data reveal an unexpected function of mTORC1 in suppressing IMLEC expansion. The high vulnerability to TLR ligands after IMLEC expansion highlights a new consequence of defective hematopoiesis and a new mechanism of immune tolerance.

Two groups have previous reported that inactivation of mTORC1 by deletion of *Rptor* leads to massive accumulation of $CD11b^{+}Gr\text{-}1^{-}$ cells in the BM [32-33]. Similar results were obtained in mice with *Mtor* deletion in the hematopoietic cells [48]. We have demonstrated here that despite expression of a myeloid cell marker CD11b, the $CD11b^{+}Gr\text{-}1^{-}$ BM cells have lymphoid morphology. The active production of sterile transcripts at Ig loci suggests that these cells have partially

committed to the B-cell lineage, while lack of VDJ rearrangement and cell surface B cell markers suggest that the differentiation toward the B cell lineage is limited. Importantly, this cell population expresses high levels of PD-L1 but does not express markers for other lymphoid cells including T cells (CD3) and NK cells (NK1.1) as well as for myeloid cells including F4/80, Gr-1 and CD115. Expression of CD11b also distinguishes IMLECs from ILCs [41], which are $CD11b^-$. PCA analysis demonstrated that IMLECs are distinct from but close to B cells and macrophages in gene expression profiles. While at much lower frequencies, cells with the same phenotypes and functional properties were also identified in normal BM, peripheral lymphoid and non-lymphoid organs.

It is of interest to note that the hallmark of IMLECs is the high expression of cell surface PD-L1. First identified as B7-H1 [49], PD-L1 has been shown to be involved in tumor evasion of T cell immunity, both by inducing exhaustion of effector T cells and by shielding tumor cells from effector T cells [50-51]. With the induction by cytokines such as IFN-γ and hypoxic tumor microenvironment, PD-L1 has been found on both tumor cells and host inflammatory cells such as myeloid derived DCs [52-53], tumor-infiltrating myeloid derived suppressor cells [54]. Recent studies have demonstrated that PD-L1 is an important biomarker and therapeutic target in cancer immunotherapy [55-56]. Since IMLECs constitutively express high levels of PD-L1, it will be of interest to investigate their function in cancer immunity. It's worth noting that IMLECs of Raptor-deficient BM have an overall higher expression of PD-L1 than that of Raptor-sufficient BM, perhaps this

reflects the indirect consequence of reduced mTORC1-mediated translation of PD-L1 negative regulators.

Since the IMLEC population expanded at the expense of granulocytes in the BM, we tested if IMLECs were derived by trans-differentiation of the granulocytes. Our genetic analyses demonstrated that inactivation of mTORC1 in the granulocytes, using *Lyz2-Cre*, failed to produce this subset, suggesting that loss of mTORC1 in granulocytes does not cause their trans-differentiation into IMLECs. Furthermore, since inactivation of mTORC1 in $CD11b^{+}Gr\text{-}1^{+}$ granulocytes did not affect their abundance in BM, loss of granulocytes in the mice with broad deletion of *Rptor* in all hematopoietic cells was not due to a cell-intrinsic requirement for mTORC1 in survival of granulocytes. Since IMLECs generally do not undergo active proliferation and are prone to apoptosis, their massive accumulation is most likely due to continuous production rather than self-renewal. Indeed, while LSKs and CMPs differentiate into IMLECs both *in vitro* and *in vivo*, IMLECs are not able to propagate *in vivo* (data not shown). Since *Lyz2-Cre* mediated *Rptor* deletion does not result in accumulation of IMLECs, it is obvious that IMLEC differentiation pathway is initiated before *Lyz2-Cre* expression which also occurs in some CMPs, and not all CMPs can give rise to IMLEC. On the other hand, since CLPs give rise to IMLEC *in vitro*, the possibility that other progenitor cells may give rise to IMLECs has not been ruled out.

Since heterozygous mutation of *Myb* causes an increase of $CD11b^{+}Gr\text{-}1^{low/-}$ cells in BM [42], we tested if conditional deletion of *Myb* is sufficient to cause accumulation of IMLEC. Our data demonstrate that cell-intrinsic reduction of *Myb* in BM resulted in accumulation of $CD11b^{+}$ $Gr\text{-}1^{-}$ $PD\text{-}L1^{+}$ IMLECs. It is of interest to note that mice with inactivation of *Rptor* share many hematopoietic phenotypes with mice harboring targeted disruption of *Myb*, such as an increase in HSPCs [57] and defective B-lymphopoiesis[58-60]. Moreover, consistent with the proposed roles of c-Myb in regulating precise hematopoietic commitments, CMPs with deletion of either *Rptor* or *Myb* favored differentiation to $CD11b^{+}$ $Gr\text{-}1^{-}$ cells [61]. Since our data show that the majority of the $CD11b^{+}Gr\text{-}1^{-}$ cells generated from CMPs are IMLECs, these data support the notion that IMLEC accumulation in *Rptor* cKO BM is caused by reduced *Myb* expression in CMPs.

While the mechanism by which mTORC1 down-regulates *Myb* remains to be fully elucidated, we have found a general up-regulation of putative miRNAs targeting *Myb* in HSPCs after *Rptor* deletion. Our data suggest that mTORC1 inactivation in HSPCs expands IMLECs by down-regulation of *Myb*, perhaps through increased miRNA biogenesis.

Previous studies by us and others have demonstrated a critical role for regulated mTOR signaling in hematopoiesis [27-28, 62]. Thus, while mTOR activation by deletion of *Tsc1* complex expands the numbers of hematopoietic stem cells, it causes reduced hematopoietic stem cell function but induced leukemic stem cells in conjunction with *Pten* deletion. This is consistent with the generally accepted

association between defective differentiation and leukemiogenesis, which forms the foundation for treatment of leukemia through induction of differentiation [63]. The expansion of IMLECs caused by mTORC1 inactivation did not lead to leukemiogenesis as IMLECs are non-dividing cells that undergo a high rate of apoptosis. Instead, our data demonstrate a new consequence of defective differentiation, namely generation of a new population of cells with distinct effector function, as discussed below.

Our RNA-seq data suggest that IMLECs broadly over-express pattern recognition receptors for innate immunity. Corresponding to a broad, although not universal TLR elevation, IMLECs mount drastically exacerbated responses to all TLR ligands tested *in vitro*. Intracellular cytokine staining revealed that both normal and *Rptor*-cKO IMLECs were among the most active producers of inflammatory cytokines. Surprisingly, although *Rptor*$^{-/-}$ BM cells have normal TLR5 levels, they produce 10-20 fold more inflammatory cytokines, such as TNF-α and MCP-1 in response to TLR5 ligand. It is therefore likely that beyond TLRs, IMLECs have acquired other features that enhance their response to TLR ligands.

Apart from BM, expanded IMLECs are broadly distributed in lymphoid and non-lymphoid organs such as lung and liver. Our data demonstrate that an increase in IMLEC numbers makes the host highly vulnerable to TLR ligands such as LPS and polyI:C, as indicated by rapid demise of mice following pIpC and low doses of LPS injections. Since necrosis of normal tissues leads to release of

endogenous TLR ligands, such as HMGB1[47] and HSP70 [64], and since unregulated host response to HMGB1 leads to fatal inflammation[11], it is conceivable that expansion of IMLECs may also make the host more vulnerable to tissue injury- induced inflammation. This is evidenced by elevated inflammation in acetaminophen-triggered liver necrosis model.

The severe pathological consequences may explain the paradoxical functions of mTOR in regulation of inflammation. While mTOR signaling is known to be activated by inflammatory cytokines [65] and rapamycin has been shown to inhibit production of inflammatory cytokines [66], perhaps through its inhibition of mTOR-mediated NFκB activation [67], rapamycin has been shown to induce inflammation in a small number of transplantation patients [68-70]. Likewise, we have observed that rapamycin increases production of inflammatory cytokines in autoimmune Scurfy mice and in mice treated with high doses of endotoxin [65]. It would be of great interest to determine if rapamycin can expand IMLECs in transplantation patients and in mice that either receive high doses of endotoxin or are genetically predisposed to autoimmune disease. It is also reported that persistent mTORC1 inhibition can result in elevated inflammation, activation of STAT3 and enhanced hepatocellular carcinoma development [71]. Our findings focused on characterizing IMLECs and inflammation support the provocative findings of this report, and might provide alternative and complementary explanations. However, despite an extensive effort, we have failed to induce IMLECs by mTOR kinase inhibitor Torin2 or rapamycin in WT mice (data not shown). Therefore, under normal

circumstances, pharmaceutical inhibition of mTORC1 alone cannot achieve comparable levels of inflammation as those achieved by genetic inactivation of either *Mtor* or *Rptor*. Additional conditions must be met for mTOR inhibitors to cause inflammation. While these unknown barriers have ensured safety of mTOR inhibitors in most circumstances, their breakdown may explain paradoxical induction of inflammation by rapamycin.

The concept of immune tolerance has traditionally been reserved for adaptive immunity to avoid autoimmune diseases. A multitude of mechanisms, including clonal deletion [22-23, 72], clonal anergy [2, 73] and dominant regulatory T cells [3], have been described to reduce self-reactive T and B cell clone sizes to avoid autoimmune diseases. On the other hand, innate immunity is known to be regulated at levels of cellular activation [74] and cellular recruitment [75]. However, we and others have reported that innate immune effectors, especially NK cells, have features of adaptive immunity as their immune protective function against cancer and viruses is amplified through increased population sizes [76-77]. However, a regulatory mechanism to control innate effector population size for the sake of preventing self-destruction has not been described. Our discovery of a developmentally regulated mechanism to control the population size of IMLECs to avoid unwanted self-destruction, as described herein, reveals a parallel between adaptive and innate immunity to avoid potentially life-threatening inflammation and tissue damage. It is therefore of interest to consider the concept of immune tolerance in the area of innate immunity.

An important consideration is whether IMLEC is a normal population of hematopoietic cells or a population that arises after pathogenic mutations. While we have identified cells of similar phenotypes and functional properties in normal mice, they are extremely rare and thus have no obvious physiological functions unless they are substantially expanded. We have demonstrated that these cells do not undergo proliferation and are prone to apoptosis, and that their expansion depends on abnormal hematopoiesis. Therefore, the pathological consequence observed herein is only known to manifest itself if the mTORC1-MyB pathway is genetically inactivated, resulting in disruption of normal hematopoiesis. Further studies are needed to identify conditions that can lead to accumulation of IMLEC short of these known mutations.

In summary, our data demonstrate that inactivation of mTORC1 in hematopoietic stem/progenitor cells leads to generation of IMLECs, a new cell population that shares features with myeloid and lymphoid lineages. The greater than 500-fold increase in population size of IMLECs in mTORC1- or MyB-defective BM highlights the critical role for mTORC1 and MyB in repressing the development of sufficient number of IMLECs to cause serious inflammation and tissue damage. Our study reveals a new consequence of defective hematopoiesis and may help to extend the concept of immune tolerance to innate immunity.

Materials and Methods

Key Resources Table

Reagent type (species) or resource	Designation	Source or reference	Identifiers	Additional information
strain, strain background (*Mus musculus,C57BL/6*)	*Rptor*$^{F/F}$	PMID: 19046572		
strain, strain background (*Mus musculus,C57BL/6*)	*Myb*$^{F/F}$; *Myb*$^{F/F}$,*Rag2*$^{-/-}$,*CreER*	PMID: 15195090; PMID: 16169500		
strain, strain background (*Mus musculus,C57BL/6*)	*Mx1-Cre*	The Jackson Laboratory	Stock No: 003556; RRID:IMSR_JAX:003556	
strain, strain background (*Mus musculus,C57BL/6*)	*CreER*	The Jackson Laboratory	Stock No: 007001; RRID:IMSR_JAX:007001	
strain, strain background (*Mus musculus,C57BL/6*)	*Lyz2-Cre*	The Jackson Laboratory	Stock No: 004781; RRID:IMSR_JAX:004781	

Mice and induction of gene deletion

Rptor $^{F/F}$ mice [78] were crossed to the C57BL/6 background for more than 10 generations. *Myb* $^{F/F}$ and *Myb* $^{F/F}$*, Rag2*$^{-/-}$, *CreER* mice were reported previously[58-59, 79]. The interferon-inducible *Mx1-Cre* transgenic mice (RRID:IMSR_JAX:003556) [35], tamoxifen-inducible *Cre-ER*^{T2} transgenic mice (RRID:IMSR_JAX:007001) [80] and *Lyz2-Cre* knock-in mice (RRID:IMSR_JAX:004781) [81] with C57BL/6 background were purchased from the Jackson Laboratory. *Rptor* $^{F/F}$ mice were crossed with *Mx1-Cre* mice, *Lyz2-Cre* mice or *CreER* mice to produce *Rptor* $^{F/F}$*, Mx1-Cre* (cKO) mice, *Rptor* $^{F/F}$, *Lyz2-Cre*$^{+/+}$ mice or *Rptor*$^{F/F}$, *CreER* mice, respectively. *Myb* $^{F/F}$ mice were crossed with *Mx1-Cre* mice to generate *Myb*$^{F/F}$ (Ctrl) and *Myb*$^{F/F}$, *Mx1-Cre* (cKO) mice. Offspring of these mice were genotyped by PCR-based assays with genomic DNA from mouse tail snips. Mice were cared for in the Unit of Laboratory Animal Medicine (ULAM) at the University of Michigan, where these studies were initiated, or Research Animal Facility (RAF) of Children's National Medical Center,

where the studies were completed. All procedures involving experimental animals were approved by the University Committee on the Use and Care of Animals (UCUCA) at the University of Michigan or Children's National Medical Center.

Raptor Ctrl and cKO mice used in each experiment were sex-matched littermates. Mice were given 2 mg/kg body weight of pIpC (GE Healthcare Life Sciences) or 400μg pIpC (Sigma-Aldrich) every other day for consecutive 3 to 7 times as specified by intra-peritoneal (i.p.) injection to induce Cre expression as in previous study [82]. Deletion of target genes were confirmed as previously described[78-79]. Wild type C57BL/6 (CD45.2) mice and congenic C57BL/6 (CD45.1) mice were purchased from the Charles River Laboratories. Tamoxifen (Sigma-Aldrich) was dissolved in corn oil (Sigma-Aldrich) to 20 mg/ml and injected i.p. at 150 mg/kg/day for 5 consecutive days.

Histology, cytology and complete blood cell count

Ctrl and cKO mice were euthanized by CO_2 inhalation on day 30 of last pIpC treatment. For histology, tissues were fixed in 10% neutral buffered formalin for 24-48 hours and the sternums were then decalcified in Immunocal (formic acid-based decalcifier, Decal, Tallman, NY) for 24 hours. Tissues were trimmed and cassetted and processed to wax on an automated processor using standard methods. Sections were cut at 5 μm thickness and hematoxylin and eosin-stained slides prepared on an automated stainer. For cytology, BM was collected

from the femoral marrow cavity with a fine diameter paintbrush dipped in sterile PBS with 5% fetal bovine serum and cytology smears were prepared by gently brushing the collected cells in parallel lines on a glass slide. Cytology slides of BM smear and cytospins of FACS-sorted BM cells were stained using a Romanowsky-based stain (Diff-Quik, Hema 3 Manual staining system, Fisher Scientific).

Histological and cytological parameters were evaluated using an Olympus BX45 light microscope at total magnifications ranging from 40 X to 100 X (oil). Histological alterations were descriptively identified. Cytological alterations were descriptively identified and quantitative BM differential counts were made using a manual differential counter and standard criteria for cell identification. Images were taken using a 12.5 megapixel microscope-mounted Olympus DP72 digital camera and accompanying software (Olympus). Complete blood cell count was performed using the Hemavet 950 Hematology System (Drew Scientific Inc.) by the Animal Diagnostic Laboratory of ULAM Pathology Cores for Animal Research in the University of Michigan.

Cells preparation and bleeding

BM cells were flushed out from the long bones (tibiae and femurs) by a 25-gauge needle with staining buffer (1XHanks Balanced Saline Solution without calcium or magnesium, supplemented with 2% heat-inactivated fetal bovine serum). Single cell suspensions of spleen, thymus, lung and lymph nodes were generated by

gently squashing with frosted slides in a small volume of staining buffer. Cells from mouse peritoneal cavity were harvested as described before[83]. For isolation of mouse liver mononuclear cells, liver fragments were pressed through 70μm round cell strainer (Becton Dickinson). Single-cell suspensions in a 35% Percoll solution (GE Healthcare) were centrifuged for 20 minutes at 800g with brake off at room temperature. Pellet was collected and washed with staining buffer. Peripheral blood was collected by retro-orbital bleeding with heparinized capillary tubes or by submandibular bleeding with a lancet.

Flow cytometry

For surface staining, cells were stained with the indicated antibodies (Abs) in staining buffer for 20 minutes at 4 °C. In the characterization of surface markers for $CD11b^{+}$ $Gr\text{-}1^{-}$ cells, Fcγ receptors were pre-blocked by incubating cells with culture medium from hybridoma 2.4G2 [84] for 20 minutes at 4°C. For intracellular staining, cells were first stained with the indicated surface markers Abs and then fixed with Cytofix/Cytoperm buffer (BD Biosciences) for 1-2 hours at 4°C, followed by incubation with Cytoperm Plus buffer (BD Biosciences) for 15 minutes at room temperature (R.T.). After refixing for 15 minutes at R.T., cells were incubated with antibodies or isotype controls for 20 minutes (anti-TNF/IgG, anti-Ki-67Abs) or overnight (anti-c-Myb/IgG Abs) and further stained with the secondary Ab if necessary. BrdU labeling experiments were performed per the manufacture's instruction (BD Biosciences), as previously reported [29, 82]. Apoptosis assays by 7-AAD and Annexin V (BD Biosciences) were according to

711 manufacturer's instructions. All FACS analyses were performed on a BD LSR II
712 or a Canto II Flow Cytometer, and data were analyzed with FlowJo software
713 (Tree Star, Inc.). The enrichment of Lin^- BM cells was performed using MACS
714 beads from mouse Lineage Cell Depletion Kit (Miltenyi Biotec). $CD11b^+$ $Gr\text{-}1^-$ BM
715 cells from *Rptor* $^{F/F}$*, Mx1-Cre* mice, Lin^- $CD11b^+$ $PD\text{-}L1^+$ IMLECs / LSK / CLP /
716 CMP populations from Raptor Ctrl/cKO or WT mice, $CD11b^+$ $Gr\text{-}1^+$ / $CD11b^-$ $Gr\text{-}1^-$
717 BM populations from *Rptor* $^{F/F}$*, Lyz2-Cre*$^{+/+}$ mice, $CD11b^{high}$ $Gr\text{-}1^-$ $F4/80^+$
718 peritoneal macrophages were sorted using FACSAria II or Influx™ cell sorter
719 (BD Biosciences). The detailed information on Abs used in this study is in
720 **Supplementary file 3.**
721
722 **BM cells transplantation**
723 C57BL/6 Ly5.2 ($CD45.1^+$) recipient mice at the age of 6-12 weeks old were
724 lethally irradiated for total 900-1,100 rads with a Cs-137 γ-ray source or a RS
725 2000 X-ray irradiator (Rad Source Technologies, Inc.). Indicated donor BM cells
726 (whole BM or FACS-sorted BM cells) were transplanted into recipients through
727 the mice tail by intra-venous (i.v.) injection within 24 hours after irradiation [82]. At
728 different time points post-transplantation, peripheral blood from the recipient mice
729 was analyzed by flow cytometry to test the reconstitutions.
730
731 **Conventional PCR and quantitative PCR**
732 Genomic DNA was isolated from BM cells by DNeasy Blood and Tissue Kit
733 (Qiagen) as per manufacturer's instructions. Total RNA was isolated using TRIzol

(Invitrogen) or ReliaPrep™ RNA Cell Miniprep System (Promega). Reverse transcription was carried out using random hemaxmer primers and SuperScript II Reverse Transcriptase (Invitrogen). Conventional PCR was performed using GoTaq Green Master Mix (Promega). Quantitative PCR (q-PCR) was performed by the 7500 real-time PCR system using Power SYBR Green Master Mixture (Applied Biosystems). Fold changes were calculated according to the ΔΔCT method [85]. The primers used for conventional PCR and q-PCR are listed in **Supplementary file 4**.

Ig gene rearrangement test by V(D)J analysis

Immunoglobulin (Ig) gene recombination was determined using genomic DNA as previously described [86]. For Heavy chain, a semi-nested PCR strategy was employed to amplify the framework regions of VH to specific sites of JH. First round amplification of 25 cycles was performed with primers FR/JH1 (70°C annealing/ 20 sec extension). Second round amplification of 35 cycles was with primers FR/JH2 (65°C annealing/ 30 sec extension). Light chain (I*gk* and *Igl*) recombination was tested by primers V_κ /J_κ5 and V_λ1 /J_λ1,3 following previous report [87]. Sequences of primers used are listed in **Supplementary file 4**.

OP9 cell co-culturing with HSPCs

OP9 stromal cell line (ATCC Cat# CRL-2749, RRID:CVCL_4398) was purchased from American Type Culture Collection (ATCC, Manassas, USA). No cell lines used in this study were listed in the database of cross-contaminated or

misidentified cell lines suggested by International Cell Line Authentication Committee (ICLAC). All cell lines from ATCC were authenticated by the STR profiling method and tested as mycoplasma contamination free by ATCC. OP9 cells were maintained in α-MEM medium (Life Technologies) supplemented with 20% heat-inactivated fetal bovine serum (Hyclone), 100 units/ml of penicillin and 100 µg/ml of streptomycin (Gibco). The 6-well and 12-well flat-bottomed plates were pre-coated with OP9 cells at approximate 100% confluence after overnight growth. Subsequently $2X10^3$ LSK (Lin^- c-Kit^+ $Sca\text{-}1^+$) or $5X10^4$ CMP (Lin^- c-Kit^+ $Sca\text{-}1^-$ $CD34^{Medium}CD16/32^{Medium}$) cells or $5X10^4$ CLP (Lin^- $CD127^+$c-Kit^{Medium} $Sca\text{-}1^{Medium}$) cells FACS-sorted from Raptor Ctrl/cKO BM were seeded. The co-culturing medium was additionally supplemented with 2ng/ml murine recombinant IL-3, 2ng/ml murine recombinant IL-6, 20ng/ml murine recombinant SCF, 10ng/ml murine recombinant Flt3L and 5ng/ml murine recombinant IL-7 (all from R&D Systems). Lenti viral particles were produced in HEK 293T cells (ATCC Cat# CRL-3216, RRID:CVCL_0063) by transiently co-transfecting control vector pWPI (Plasmid #12254, Addgene), or pWPI-Myb (cDNA of *Myb* was purchased from Dharmacon™ of GE Lifesciences, Catalog Number: MMM1013-202763262; Clone ID: 3672769) together with helper plasmids pMD2.G (Plasmid #12259, Addgene) and psPAX2 (Plasmid #12260, Addgene) using FuGENE® HD Transfection Reagent (Promega). OP9 cells were replaced every 3-4 days by transferring co-culturing cells to new plates pre-coated with fresh OP9 cells. The hematopoietic cells in suspension were harvested on day 10-14 post seeding and subjected to flow cytometric analyses.

TLR stimulation and inflammatory cytokine assay

For *in vitro* TLR stimulation, fresh BM cells were seeded in a 12-well plate with a density of $4X10^6$ cells/ well(1ml medium/well) or in a 48-well plate with a density of $1X10^6$ cells/ well (200µl medium/well). The culture medium was RPMI 1640 (Life Technologies) supplemented with 10% heat-inactivated fetal bovine serum (Hyclone), 100 units/ml of penicillin and 100 µg/ml of streptomycin (Gibco). BM cells were stimulated with 1µg/ml LPS (Sigma-Aldrich, from O111:B4 *E.coli*) or a panel of TLR agonists (InvivoGen) for 16 hours. For intracellular cytokine staining, the protein transport inhibitor Brefeldin A (eBioscience) was added to the culturing medium during the last 4 hours of incubation.

The concentrations of the TLR agonists for *in vitro* studies were as following: TLR1/2-Pam3CSK4, 300ng/ml; TLR2-HKLM, 10^8 cells/ml; TLR3-pIpC(HMW), 10µg/ml; TLR4-LPS-EK, 1µg/ml; TLR5-FLA-ST, 1µg/ml; TLR6/2-FSL-1, 100ng/ml; TLR7-ssRNA-DR/LyoVec, 1µg/ml; TLR9-ODN1826, 1µM. For *in vivo* tests, pIpC (GE Healthcare, 2 mg/kg), LPS (from O55:B5 *E.coli*, Sigma-Aldrich, 5 mg/kg) and Acetaminophen (Children's TYLENOL, 3.2 mg/mouse) were injected i.p. Supernatant from *in vitro* cultured BM cells and serum from *in vivo* treated mice were assayed for inflammatory cytokines by BD Cytometric Bead Array (CBA)-Mouse Inflammation Kit according to the manufacturer's protocols.

cDNA library preparation and RNA sequencing

803 FACS-sorted CD11b^{+} Gr-1^{-} BM cells from Raptor cKO mice and whole BM cells
804 from Raptor Ctrl mice were used for RNA isolation with TRIzol Reagent (Life
805 Technologies) per manufacturer's instructions. The cDNA libraries were
806 constructed following the standard Illumina protocols by TruSeq RNA and DNA
807 sample preparation kits (Illumina). Briefly, beads containing oligo (dT) were used
808 to isolate poly(A) mRNA from total RNA. Purified mRNA was then fragmented in
809 fragmentation buffer. Using these short fragments as templates, random
810 hexamer-primers were used to synthesize the first-strand cDNA. The second-
811 strand cDNA was synthesized using buffer, dNTPs, RNase H and DNA
812 polymerase I. Short double-stranded cDNA fragments were purified for end
813 repair and the addition of an 'A' base. Next, the short fragments were ligated to
814 Illumina sequencing adaptors. DNA fragments of a selected size were gel-
815 purified and amplified by PCR. The amplified cDNA libraries were quality
816 validated and then subjected to 50 nt single-end sequencing on an Illumina
817 HiSeq 2000 at the University of Michigan DNA Sequencing Core.
818
819 **RNA-seq gene expression analysis**
820 The reference sequences used were genome and transcriptome sequences
821 downloaded from the UCSC website (version mm10). Clean reads were
822 respectively aligned to the reference genome and transcriptome using Tophat
823 (RRID:SCR_013035)[88]. No more than 2 mismatches were allowed in the
824 alignment for each read. Reads that could be uniquely mapped to a gene were
825 used to calculate the expression level. The gene expression level was measured

by the number of uniquely mapped reads per kilobase of exon region per million mappable reads (RPKM) and was calculated by DEGseq (RRID:SCR_008480)[89].

$$\mathrm{RPKM} = \frac{10^6\ \mathrm{C}}{\frac{\mathrm{NL}}{10^3}}$$

The formula was defined as below:

in which C was the number of reads uniquely mapped to the given gene; N was the number of reads uniquely mapped to all genes; L was the total length of exons from the given gene. For genes with more than one alternative transcript, the longest transcript was selected to calculate the RPKM.

PCA, differential and cell-specific expression analysis

The RPKM method eliminates the influence of different gene lengths and sequencing discrepancies on the gene expression calculation. Therefore, the RPKM value can be used for comparing the differences in gene expression among samples. The RPKM value of all RNA-seq raw data were calculated according to the same workflow as stated above.

A function was implemented in the R software to perform principal component analysis (PCA). This function computes the eigenvalues and eigenvectors of the dataset (23498 genes) using the correlation matrix. The eigenvalues were then ordered from highest to lowest, indicating their relative contribution to the structure of the data. The projection of each sample defined by components was represented as a dot plot to generate the PCA figures.

Selected samples were then pooled by subtypes and a two sided t-test with FDR (False discovery rate) of 0.05 and fold change of 4 was performed to identify differentially expressed genes between IMLECs and other subtypes (mean RPKM values of genes in two subtypes both below 5 were deleted). For subtype-specific genes identified, a one-sided t-test (null hypothesis is greater) was performed with FDR of 0.01 and fold change of 4 contrasting each subtype in turn versus all other subtypes pooled, and statistically significant genes were assigned to the respective subtype signature.

RNA-seq datasets in this study have been deposited in the Gene Expression Omnibus (GEO) database as accession number GSE67863. Other public RNA-seq datasets used are as followings: peritoneal $CD11b^{+}F4/80^{+}$ macrophages (GSM1103013, GSM1103014 in GEO Series GSE45358); normal BM $CD11b^{+}$ $Gr\text{-}1^{+}$ granulocytes (GSM1166354, GSM1166355, GSM1166356 in GEO Series GSE48048); BM-derived dendritic cells (GSM1012795, GSM1012796 and GSM1012797 in GEO Series GSE41265); BM erythroid cells (GSM1208164, GSM1208165 and GSM1208166 in GEO Series GSE49843); BM pro B and pre B cells (GSM978778 and GSM978779 in GEO Series GSE39756); Naïve B cells (GSM1155172, GSM1155176, GSM1155180 and GSM1155184 in GEO Series GSE47703); activated B cells (GSM1155170, GSM1155174, GSM1155178 and GSM1155182 in GEO Series GSE47703); CD4 T cells, CD8 T cells and natural regulatory T (nTreg) cells (GSM1169492, GSM1169501, GSM1169493, GSM1169502, GSM1169499 and GSM1169508 in GEO Series GSE48138); .

Spleen NK cells (GSM1257953, GSM1257954, GSM1257955 and GSM 1257956 in GEO Series GSE52047); Blood neutrophils (GSM1340629, GSM1340630, GSM1340631 and GSM1340632 in GEO Series GSE55633); Lung basophils and eosinophils (GSM1358432, GSM1358433, GSM1358436 and GSM1358437 in GEO Series GSE56292). RNA-seq data on *ex vivo* DC subsets are obtained from GEO Series GSE62704: GSM1531794 (CDP), GSM1531795 (pDC), GSM1531796 (preDC), GSM1531797 (DN DC), GSM1531798 ($CD4^+$ DC), GSM1531799 ($CD8^+$ DC).

Genome browser display of immunoglobulin expression

To facilitate the global viewing of transcript structure and gene expression quantity of immunoglobulin, an interface in which RNA-seq gene expression of immunoglobulin can be viewed in Genome Browser display was constructed. For viewing and analysis, the UCSC Genome Browser (http://www.genome.ucsc.edu, RRID:SCR_005780) [90] with the mm10 version of the mouse genome was used. For each base in each cell type, the normalized number of aligned reads count was defined as below:

$$\text{Normalized number of aligned reads count} = \mathrm{A} * \frac{\sum_{k=0}^{n} N_k}{\mathrm{n}}$$

in which N was the number of reads uniquely mapped to the given base in each cell type ; n was the number of replicates for each cell type samples; A was a constant t in which takes the value of 3.5E+7. The normalized number of aligned reads count for each base in each cell type was stored as WIG file and was

uploaded to UCSC genome browser. For each track, y-axis depicted the normalized number of aligned reads count and x-axis depicts physical distance in bases along the chromosome.

Statistical analysis

All the data are presented as mean ± SD. Unless otherwise indicated, two-tailed, unpaired student's *t* tests were used for comparison between two experimental groups. In Figure 8I and Figure 8J, where the data do not follow normal distribution, Mann-Whitney tests were used. The log-rank tests were used for the Kaplan-Meier survival analysis. Statistical significance was determined as $p<0.05$ (*, $p<0.05$; **, $p<0.01$; ***, $p<0.001$).

Acknowledgements

We thank Dr. Hans Schreiber (University of Chicago) and all the colleagues in our laboratory for their helpful discussions, and Ms. Morgan E. Daley for editorial assistance. This work was supported by the grants from National Institute of Health AG036690, AI64350, CA183030 and CA171972. This work was initiated at the University of Michigan then completed at Children's Research Institute of Children's National Medical Center.

References

1. Burnet, F.M. A modification of Jerne's theory of antibody production using the concept of clonal selection. *Aust. J. Sci.* **20**, 67-69 (1957).
2. Nossal, G.J. & Pike, B.L. Clonal anergy: persistence in tolerant mice of antigen-binding B lymphocytes incapable of responding to antigen or mitogen. *Proc. Natl. Acad. Sci. U. S. A.* **77**, 1602-1606 (1980).
3. Sakaguchi, S., Sakaguchi, N., Asano, M., Itoh, M. & Toda, M. Immunologic self-tolerance maintained by activated T cells expressing IL-2 receptor alpha-chains (CD25). Breakdown of a single mechanism of self-tolerance causes various autoimmune diseases. *J. Immunol.* **155**, 1151-1164 (1995).
4. Janeway, C.A. Approaching the asymptote? Evolution and revolution in immunology. *Cold Spring Harb. Symp. Quant. Biol.* **54**, 1-13 (1989).
5. Medzhitov, R., Preston-Hurlburt, P. & Janeway, C.A., Jr. A human homologue of the Drosophila Toll protein signals activation of adaptive immunity. *Nature* **388**, 394-397 (1997).
6. Liu, Y. & Janeway, C.A., Jr. Microbial induction of co-stimulatory activity for CD4 T-cell growth. *Int. Immunol.* **3**, 323-332 (1991).
7. Liu, Y. & Janeway, C.A.J. Cells that present both specific ligand and the costimulatory activity are the most efficient inducer of clonal expansion of normal CD4 T cells. *Proc Natl Acad Sci USA* **89**, 3845-3849 (1992).
8. Wu, Y. & Liu, Y. Viral induction of co-stimulatory activity on antigen-presenting cells bypasses the need for CD4+ T-cell help in CD8+ T-cell responses. *Curr. Biol.* **4**, 499-505 (1994).
9. Pasare, C. & Medzhitov, R. Control of B-cell responses by Toll-like receptors. *Nature* **438**, 364-368 (2005).
10. Stetson, D.B., Ko, J.S., Heidmann, T. & Medzhitov, R. Trex1 prevents cell-intrinsic initiation of autoimmunity. *Cell* **134**, 587-598 (2008).
11. Chen, G.Y., Tang, J., Zheng, P. & Liu, Y. CD24 and Siglec-10 selectively repress tissue damage-induced immune responses. *Science* **323**, 1722-1725 (2009).
12. Liu, Y., Chen, G.Y. & Zheng, P. CD24-Siglec G/10 discriminates danger- from pathogen-associated molecular patterns. *Trends Immunol* **30**, 557-561 (2009).
13. Liu, Y., Chen, G.Y. & Zheng, P. Sialoside-based pattern recognitions discriminating infections from tissue injuries. *Curr. Opin. Immunol.* (2010).
14. Ljunggren, H.G. & Karre, K. In search of the 'missing self': MHC molecules and NK cell recognition. *Immunol. Today* **11**, 237-244 (1990).
15. Liew, F.Y., Xu, D., Brint, E.K. & O'Neill, L.A. Negative regulation of toll-like receptor-mediated immune responses. *Nat Rev Immunol* **5**, 446-458 (2005).
16. Takeuchi, O. & Akira, S. Pattern recognition receptors and inflammation. *Cell* **140**, 805-820 (2010).
17. Anderson, M.S. *et al.* Projection of an immunological self shadow within the thymus by the aire protein. *Science* **298**, 1395-1401 (2002).
18. Gao, J.-X. *et al.* Perinatal blockade of B7-1 and B7-2 inhibits clonal deletion of highly pathogenic autoreactive T cells. *J. Exp. Med.* **195**, 959-971 (2002).

19. Hori, S., Nomura, T. & Sakaguchi, S. Control of regulatory T cell development by the transcription factor Foxp3. *Science* **299**, 1057-1061 (2003).
20. Fontenot, J.D., Gavin, M.A. and Rudensky, A.Y.. Foxp3 programs the development and function of CD4+CD25+ regulatory T cells. *Nat Immunol.* **4**, 330-334 (2003).
21. Nemazee, D.A. & Burki, K. Clonal deletion of B lymphocytes in a transgenic mouse bearing anti-MHC class I antibody genes. *Nature* **337**, 562-566 (1989).
22. Sha, W.C. *et al.* Positive and negative selection of an antigen receptor on T cells in transgenic mice. *Nature* **336**, 73-76 (1988).
23. Kisielow, P., Bluthmann, H., Staerz, U.D., Steinmetz, M. & von Boehmer, H. Tolerance in T-cell-receptor transgenic mice involves deletion of nonmature CD4+8+ thymocytes. *Nature* **333**, 742-746 (1988).
24. Metcalf, D. Cellular hematopoiesis in the twentieth century. *Semin. Hematol.* **36**, 5-12 (1999).
25. Weissman, I.L. Developmental switches in the immune system. *Cell* **76**, 207-218 (1994).
26. Inoki, K., Li, Y., Zhu, T., Wu, J. & Guan, K.L. TSC2 is phosphorylated and inhibited by Akt and suppresses mTOR signalling. *Nat Cell Biol* **4**, 648-657 (2002).
27. Yilmaz, O.H. *et al.* Pten dependence distinguishes haematopoietic stem cells from leukaemia-initiating cells. *Nature* **441**, 475-482 (2006).
28. Zhang, J. *et al.* PTEN maintains haematopoietic stem cells and acts in lineage choice and leukaemia prevention. *Nature* **441**, 518-522 (2006).
29. Chen, C. *et al.* TSC-mTOR maintains quiescence and function of hematopoietic stem cells by repressing mitochondrial biogenesis and reactive oxygen species. *J Exp Med* **205**, 2397-2408 (2008).
30. Hara, K. *et al.* Raptor, a binding partner of target of rapamycin (TOR), mediates TOR action. *Cell* **110**, 177-189 (2002).
31. Kim, D.H. *et al.* mTOR interacts with raptor to form a nutrient-sensitive complex that signals to the cell growth machinery. *Cell* **110**, 163-175 (2002).
32. Hoshii, T. *et al.* mTORC1 is essential for leukemia propagation but not stem cell self-renewal. *J. Clin. Invest.* **122**, 2114-2129 (2012).
33. Kalaitzidis, D. *et al.* mTOR complex 1 plays critical roles in hematopoiesis and Pten-loss-evoked leukemogenesis. *Cell Stem Cell* **11**, 429-439 (2012).
34. Polak, P. *et al.* Adipose-specific knockout of raptor results in lean mice with enhanced mitochondrial respiration. *Cell metabolism* **8**, 399-410 (2008).
35. Kuhn, R., Schwenk, F., Aguet, M. & Rajewsky, K. Inducible gene targeting in mice. *Science* **269**, 1427-1429 (1995).
36. Sleckman, B.P., Gorman, J.R. & Alt, F.W. Accessibility control of antigen-receptor variable-region gene assembly: role of cis-acting elements. *Annu. Rev. Immunol.* **14**, 459-481 (1996).
37. Mombaerts, P. *et al.* RAG-1-deficient mice have no mature B and T lymphocytes. *Cell* **68**, 869-877 (1992).
38. Schatz, D.G., Oettinger, M.A. & Baltimore, D. The V(D)J recombination activating gene, RAG-1. *Cell* **59**, 1035-1048 (1989).

39. Shinkai, Y. *et al.* RAG-2-deficient mice lack mature lymphocytes owing to inability to initiate V(D)J rearrangement. *Cell* **68**, 855-867 (1992).
40. Oettinger, M.A., Schatz, D.G., Gorka, C. & Baltimore, D. RAG-1 and RAG-2, adjacent genes that synergistically activate V(D)J recombination. *Science* **248**, 1517-1523 (1990).
41. Walker, J.A., Barlow, J.L. & McKenzie, A.N. Innate lymphoid cells--how did we miss them? *Nat Rev Immunol* **13**, 75-87 (2013).
42. Garcia, P. *et al.* Reduced c-Myb activity compromises HSCs and leads to a myeloproliferation with a novel stem cell basis. *EMBO J.* **28**, 1492-1504 (2009).
43. Ye, P. *et al.* An mTORC1-Mdm2-Drosha axis for miRNA biogenesis in response to glucose- and amino acid-deprivation. *Mol. Cell* **57**, 708-720 (2015).
44. Betel, D., Koppal, A., Agius, P., Sander, C. & Leslie, C. Comprehensive modeling of microRNA targets predicts functional non-conserved and non-canonical sites. *Genome Biol* **11**, R90 (2010).
45. Lin, Y.C. *et al.* c-Myb is an evolutionary conserved miR-150 target and miR-150/c-Myb interaction is important for embryonic development. *Mol. Biol. Evol.* **25**, 2189-2198 (2008).
46. Xiao, C. *et al.* MiR-150 controls B cell differentiation by targeting the transcription factor c-Myb. *Cell* **131**, 146-159 (2007).
47. Scaffidi, P., Misteli, T. & Bianchi, M.E. Release of chromatin protein HMGB1 by necrotic cells triggers inflammation. *Nature* **418**, 191-195 (2002).
48. Guo, F. *et al.* Mouse gene targeting reveals an essential role of mTOR in hematopoietic stem cell engraftment and hematopoiesis. *Haematologica* **98**, 1353-1358 (2013).
49. Dong, H., Zhu, G., Tamada, K. & Chen, L. B7-H1, a third member of the B7 family, co-stimulates T-cell proliferation and interleukin-10 secretion [see comments]. *Nat. Med.* **5**, 1365-1369 (1999).
50. Hirano, F. *et al.* Blockade of B7-H1 and PD-1 by monoclonal antibodies potentiates cancer therapeutic immunity. *Cancer Res.* **65**, 1089-1096 (2005).
51. Barber, D.L. *et al.* Restoring function in exhausted CD8 T cells during chronic viral infection. *Nature* **439**, 682-687 (2006).
52. Curiel, T.J. *et al.* Blockade of B7-H1 improves myeloid dendritic cell-mediated antitumor immunity. *Nat. Med.* **9**, 562-567 (2003).
53. Dong, H. *et al.* Tumor-associated B7-H1 promotes T-cell apoptosis: a potential mechanism of immune evasion. *Nat. Med.* **8**, 793-800 (2002).
54. Noman, M.Z. *et al.* PD-L1 is a novel direct target of HIF-1alpha, and its blockade under hypoxia enhanced MDSC-mediated T cell activation. *J. Exp. Med.* **211**, 781-790 (2014).
55. Garon, E.B. *et al.* Pembrolizumab for the treatment of non-small-cell lung cancer. *N. Engl. J. Med.* **372**, 2018-2028 (2015).
56. Brahmer, J.R. *et al.* Safety and activity of anti-PD-L1 antibody in patients with advanced cancer. *N. Engl. J. Med.* **366**, 2455-2465 (2012).
57. Sandberg, M.L. *et al.* c-Myb and p300 regulate hematopoietic stem cell proliferation and differentiation. *Developmental cell* **8**, 153-166 (2005).
58. Fahl, S.P., Crittenden, R.B., Allman, D. & Bender, T.P. c-Myb is required for pro-B cell differentiation. *J Immunol* **183**, 5582-5592 (2009).

59. Thomas, M.D., Kremer, C.S., Ravichandran, K.S., Rajewsky, K. & Bender, T.P. c-Myb is critical for B cell development and maintenance of follicular B cells. *Immunity* **23**, 275-286 (2005).
60. Greig, K.T. *et al.* Critical roles for c-Myb in lymphoid priming and early B-cell development. *Blood* **115**, 2796-2805 (2010).
61. Lieu, Y.K. & Reddy, E.P. Impaired adult myeloid progenitor CMP and GMP cell function in conditional c-myb-knockout mice. *Cell Cycle* **11**, 3504-3512 (2012).
62. Chen, C. *et al.* TSC-mTOR maintains quiescence and function of hematopoietic stem cells by repressing mitochondrial biogenesis and reactive oxygen species. *J. Exp. Med.* **205**, 2397-2408 (2008).
63. Nowak, D., Stewart, D. & Koeffler, H.P. Differentiation therapy of leukemia: 3 decades of development. *Blood* **113**, 3655-3665 (2009).
64. Millar, D.G. *et al.* Hsp70 promotes antigen-presenting cell function and converts T-cell tolerance to autoimmunity in vivo. *Nat. Med.* **9**, 1469-1476 (2003).
65. Chen, C., Liu, Y. & Zheng, P. Mammalian target of rapamycin activation underlies HSC defects in autoimmune disease and inflammation in mice. *J. Clin. Invest.* **120**, 4091-4101 (2010).
66. Abraham, R.T. & Wiederrecht, G.J. Immunopharmacology of rapamycin. *Annu. Rev. Immunol.* **14**, 483-510 (1996).
67. Lee, D.F. *et al.* IKK beta suppression of TSC1 links inflammation and tumor angiogenesis via the mTOR pathway. *Cell* **130**, 440-455 (2007).
68. Diekmann, F., Andres, A. & Oppenheimer, F. mTOR inhibitor-associated proteinuria in kidney transplant recipients. *Transplant Rev (Orlando)* **26**, 27-29 (2012).
69. Thaunat, O. *et al.* Anemia after late introduction of sirolimus may correlate with biochemical evidence of a chronic inflammatory state. *Transplantation* **80**, 1212-1219 (2005).
70. Dittrich, E., Schmaldienst, S., Soleiman, A., Horl, W.H. & Pohanka, E. Rapamycin-associated post-transplantation glomerulonephritis and its remission after reintroduction of calcineurin-inhibitor therapy. *Transpl. Int.* **17**, 215-220 (2004).
71. Umemura, A. *et al.* Liver damage, inflammation, and enhanced tumorigenesis after persistent mTORC1 inhibition. *Cell Metab* **20**, 133-144 (2014).
72. Kappler, J.W., Roehm, N. & Marrack, P. T cell tolerance by clonal elimination in the thymus. *Cell* **49**, 273-280 (1987).
73. Schwartz, R.H., Mueller, D.L., Jenkins, M.K. & Quill, H. T-cell clonal anergy. *Cold Spring Harb. Symp. Quant. Biol.* **54 Pt 2**, 605-610 (1989).
74. Karre, K., Ljunggren, H.G., Piontek, G. & Kiessling, R. Selective rejection of H-2-deficient lymphoma variants suggests alternative immune defence strategy. *Nature* **319**, 675-678. (1986).
75. Springer, T.A. Traffic signals for lymphocyte recirculation and leukocyte emigration: the multistep paradigm. *Cell* **76**, 301-314 (1994).
76. Gao, J.X. *et al.* Two-signal requirement for activation and effector function of natural killer cell response to allogeneic tumor cells. *Blood* **102**, 4456-4463 (2003).

77. Sun, J.C., Beilke, J.N. & Lanier, L.L. Adaptive immune features of natural killer cells. *Nature* **457**, 557-561 (2009).
78. Bentzinger, C.F. *et al.* Skeletal muscle-specific ablation of raptor, but not of rictor, causes metabolic changes and results in muscle dystrophy. *Cell metabolism* **8**, 411-424 (2008).
79. Bender, T.P., Kremer, C.S., Kraus, M., Buch, T. & Rajewsky, K. Critical functions for c-Myb at three checkpoints during thymocyte development. *Nat Immunol* **5**, 721-729 (2004).
80. Indra, A.K. *et al.* Temporally-controlled site-specific mutagenesis in the basal layer of the epidermis: comparison of the recombinase activity of the tamoxifen-inducible Cre-ER(T) and Cre-ER(T2) recombinases. *Nucleic Acids Res* **27**, 4324-4327 (1999).
81. Clausen, B.E., Burkhardt, C., Reith, W., Renkawitz, R. & Forster, I. Conditional gene targeting in macrophages and granulocytes using LysMcre mice. *Transgenic Res.* **8**, 265-277 (1999).
82. Tang, F. *et al.* A critical role for Rictor in T lymphopoiesis. *J. Immunol.* **189**, 1850-1857 (2012).
83. Ray, A. & Dittel, B.N. Isolation of mouse peritoneal cavity cells. *J Vis Exp* (2010).
84. Kurlander, R.J., Ellison, D.M. & Hall, J. The blockade of Fc receptor-mediated clearance of immune complexes in vivo by a monoclonal antibody (2.4G2) directed against Fc receptors on murine leukocytes. *J. Immunol.* **133**, 855-862 (1984).
85. Livak, K.J. & Schmittgen, T.D. Analysis of relative gene expression data using real-time quantitative PCR and the 2(-Delta Delta C(T)) Method. *Methods* **25**, 402-408 (2001).
86. Riddell, J. *et al.* Reprogramming committed murine blood cells to induced hematopoietic stem cells with defined factors. *Cell* **157**, 549-564 (2014).
87. Cobaleda, C., Jochum, W. & Busslinger, M. Conversion of mature B cells into T cells by dedifferentiation to uncommitted progenitors. *Nature* **449**, 473-477 (2007).
88. Kim, D. *et al.* TopHat2: accurate alignment of transcriptomes in the presence of insertions, deletions and gene fusions. *Genome Biol* **14**, R36 (2013).
89. Wang, L., Feng, Z., Wang, X. & Zhang, X. DEGseq: an R package for identifying differentially expressed genes from RNA-seq data. *Bioinformatics* **26**, 136-138 (2010).
90. Kent, W.J. *et al.* The human genome browser at UCSC. *Genome Res.* **12**, 996-1006 (2002).

Figure Legends

Figure 1 Targeted mutation of *Rptor* in hematopoiesis led to massive accumulation of IMLEC.

(**A**) Schematic of experimental design. Sex-matched 6-8 weeks old Ctrl (*Rptor* $^{F/F}$) and cKO (*Rptor* $^{F/F}$*, Mx1-Cre*) mice were treated with pIpC for 7 times. The phenotypes were analyzed on day 7 or day 30 after the complement of pIpC treatment. (**B**) Representative flow cytometric analysis of myeloid cells from mice BM by CD11b and Gr-1 on day 7 after pIpC treatment. Similar data were obtained on day 30. (**C**) Frequencies of various hematopoietic cell populations in BM based on CD11b and Gr-1 markers. n=7 for Ctrl mice; n=9 for cKO mice. Data are pooled from 3 independent experiments. (**D**) Expansion of lymphoblast population in cKO BM revealed by histology. Left, H&E staining showing prominence of cells with lymphoid morphology in the cKO BM; Right, normal BM histology from Ctrl mouse showing normal myeloid and erythroid lineages. Scale bar, 20 μm. **(E)** Expansion of lymphoblast revealed by cytology. Left, cytological preparation of BM smear from cKO mouse showing preponderance of lymphocytes (short arrows) and severe depletion of myeloid and erythroid lineages. There were some promyelocytes and myelocytes present (larger cells) but no mature neutrophils. Right, normal cytological preparation of BM from Ctrl mouse. There were numerous erythroid precursors with intensely basophilic, condensed chromatin (arrowheads) and a few lymphocytes (short arrow) with less condensed chromatin. Additionally, in BM there were numerous mature neutrophils (ringed nucleus with constrictions) which were not severely depleted

in the cKO mouse. Scale bar, 10 μm. (**F**) Giemsa staining of FACS-sorted *Rptor*-deficient $CD11b^{+}Gr\text{-}1^{-}$ BM cells. Scale bar, 10μm. Similar morphology was observed in three independent experiments. (**G**) Principal component analysis (PCA) of gene expression in $CD11b^{+}$ $Gr\text{-}1^{-}$ BM cells (IMLECs) and other hematopoietic cells. Numbers along axes indicate relative scaling of the principal variables. RNA-seq data from IMLECs obtained in our study were compared with those deposited in public database by others. Datasets are from known lymphoid (Pro-B, Pre-B, Naïve B, CD4 T, CD8 T, Treg and NK) or myeloid (macrophage, dendritic cell, granulocyte, neutrophil, eosinophil, basophil and erythrocyte) subsets.

Figure 2 Unique gene signature of *Rptor* $^{-/-}$ $CD11b^{+}$ $Gr\text{-}1^{-}$ BM IMLECs. (**A**) Heat map representing the relative expression levels for indicated population-specific genes. Genes up-regulated for at least 4-fold with FDR-adjusted p-value <0.01 were considered population-specific. Numbers on right indicate amounts of population-specific genes. (**B**) Heat map representing expression levels of 48 $CD11b^{+}Gr\text{-}1^{-}$ BM IMLEC-specific genes among indicated populations including macrophage, B precursor, naive B and granulocyte. (**C**) Genome browser display of transcript structure and gene expression quantity for immunoglobulin heavy chain (IgH) complex gene region from indicated populations. For each track, the normalized numbers of aligned reads count or Reads Per Kilobase of transcript per Million mapped RNA (RPKM) are shown in y-axis, while the gene positions for the sterile transcripts are shown in x-axis. Numbers on top indicate the start

and end loci on bases along chromosome 12 for specified gene region. Similar profiles of cKO IMLEC were observed in two other samples analyzed. (**D**) mRNA levels of *Rag1* and *Rag2* in cKO $CD11b^+$ $Gr\text{-}1^-$ BM IMLECs in comparison to Ctrl whole BM cells. n=6 for Ctrl-WBM; n=8 for IMLEC. Data are pooled from 3 independent experiments. (**E**) IMLECs did not display immunoglobulin gene rearrangement. FACS-sorted $CD11b^+$ $Gr\text{-}1^-$ cells (IMLECs) from cKO BM were dissected for Ig gene rearrangement patterns of heavy chain (J_H), light chains *Igk* ($J_{L\kappa}$) and *Igl* ($J_{L\lambda}$) by PCR. WBM cells from Raptor Ctrl mice were used as positive control. These data have been repeated twice.

Figure 3 Identification of IMLEC by cell surface markers in both Raptor cKO and WT mice.

(**A**) IMLECs do not express surface markers for conventional lymphocytes (CD3, B220 and NK1.1) and stem and progenitor cells (c-Kit and Sca-1). $CD11b^+$ $Gr\text{-}1^-$ IMLECs from Raptor cKO BM were tested for their expression of lymphocytes and progenitor cell markers. These data have been repeated 3 times. (**B**) IMLECs do not express markers for monocytes and macrophages but surprisingly express high levels of PD-L1. Filled gray areas indicate distributions of fluorescence from stainings by control antibodies. One representative result of at least five experiments is shown. (**C**) *Rptor* deletion causes expansion of Lin^- ($B220^-$ $CD3^-$ $Ter119^-$ $NK1.1^-$ $Gr\text{-}1^-$ $F4/80^-$ $CD115^-$) $CD11b^+$ $PD\text{-}L1^+$ IMLECs in BM. Representative flow staining profiles for BM IMLECs (left) and their abundance summary data (right) are presented. n=5 for Ctrl BM; n=5 for cKO BM. (**D**) Lin^-

CD11b^{+} PD-L1^{+} BM IMLECs are CD11c$^{-/low}$. One representative result of two experiments is shown. (**E**) The Lin^{-} CD11b^{+} PD-L1^{+} CD11c$^{-/low}$ IMLECs are found in various lymphoid and non-lymphoid organs from WT mice. mLN, mesenteric lymph nodes; c/i LN, cervical and inguinal lymph nodes. The numbers (Mean±SD) are summarized abundances of IMLECs among mononuclear cells (MNCs) from 3 WT mice. (**F**-**H**) *Rptor* deletion caused a broad accumulation of IMLECs in lung (**F**), mesenteric lymph nodes (**G**) and peripheral (cervical and inguinal) lymph nodes (**H**). Results shown are representative of three mice in each group. (**I**) Summary data showing increased IMLECs in the peripheral blood, lymphoid and non-lymphoid organs. n=3 for both groups.

Figure 4 Comparison of IMLECs identified in both WT and Raptor-deficient BM.

(**A**) Giemsa staining of Lin^{-} CD11b^{+} PD-L1^{+} IMLECs from WT BM and *Rptor*-cKO BM. One representative result of 3 independent experiments is shown. Scale bar, 10μm. (**B**) Size and granularity of IMLECs from Raptor Ctrl and cKo BM were evaluated by FSC and SSC, respectively. n=5 for each group. (**C**) IMLEC from WT BM expresses sterile transcripts from the *Igh* and *Igl* loci. *Ig* transcript levels in macrophage are artificially defined as 1. (**D**) Heat map representing the relative expression levels for indicated population specific transcription factor genes. Genes up-regulated for at least 4-fold with FDR-adjusted p-value<0.01 were considered population-specific. (**E**) IMLECs from both WT and Raptor-cKO BM exhibited high levels of mRNA transcripts for the specified transcription

factors (*Mitf*, *Atf3* and *Zdhhc1*). n=5 for each group. (**F, G**) Ctrl and cKO IMLECs are non-cycling cells in contrast to Lin^+ BM cells. (**H, I**) IMLECs are prone to apoptosis based on their binding to Annexin V. Results in (C), (G) and (I) represent one of 2 independent experiments with each involving 3 mice per group.

Figure 5 Raptor represses differentiation of IMLEC from CMP.

(**A, B**) IMLEC accumulation in *Rptor*$^{-/-}$ BM is cell autonomous. (**A**) Diagram depicting generation of mixed BM chimera, induction of *Rptor* deletion and analyses for IMLEC. (**B**) In mixed BM chimera mice, IMLEC was accumulated only in the Raptor-deficient hematopoietic cells. Mice were sacrificed and analyzed at 4 weeks post pIpC treatment. $CD45.1^+$ and $CD45.2^+$ donor-derived BM cells were gated to show the myeloid subsets based on CD11b and Gr-1. Similar data were obtained in 3 independent experiments, each involving at least 3 mice per group. (**C, D**) BM IMLECs are not converted from $CD11b^+$ $Gr\text{-}1^-$ granulocytes. (**C**) Genotyping and deletion efficacy. $CD11b^+Gr\text{-}1^+$ cells (DP) and $CD11b^-Gr\text{-}1^-$ cells (DN) were sorted from BM of KO (*Rptor*$^{F/F}$*, Lyz2-Cre*$^{+/+}$*)* mice. Floxed and deleted *Rptor* alleles, as well as *Lyz2-Cre* wild type (WT) and mutated (MT) alleles were confirmed by PCR. (**D**) Efficient deletion of *Rptor* in the $CD11b^+Gr\text{-}1^+$ compartment failed to cause IMLEC accumulation. Data shown are representative BM flow profiles of Ctrl mice and those with *Rptor* deletion in the $CD11b^+Gr\text{-}1^+$ compartment, depicting distributions of CD11b and Gr-1 markers in adult mice. Similar data have been obtained in 3 experiments,

involving a total of 5 mice per group. (**E, F**) *Rptor*$^{-/-}$ LSK, CLP and CMP cells differentiate into IMLECs *in vitro*. (**E**) Diagram of experimental design. 2X10^3 LSK cells or 5X10^4 CLP or 5X10^4 CMP cells were co-cultured with the OP9 cells for 10 days. (**F**) *Rptor* deletion promoted generation of IMLEC. The CD45.2$^+$ leukocytes were gated and analyzed for their expression of CD11b, Gr-1 and PD-L1. Data shown are representative of three independent experiments. (**G, H**) Both LSK and CMP cells differentiate into IMLECs *in vivo*. (**G**) Diagram of BM cells transplantation. FACS-sorted, Ctrl or cKO LSK cells (5X10^4/mouse) or CMP cells (1.2 X10^5/mouse) were injected i.v. to CD45.1 recipient mice which were immediately administrated with 5 daily pIpC treatments. BM cells were harvested on day 7 for FACS analyses. (**H**) *Rptor* deletion promoted differentiation of progenitor cells into IMLEC. Donor-derived CD45.2$^+$ BM cells were gated to analyze surface markers CD11b, Gr-1 and PD-L1. Data shown are representative flow profiles from one of 3 independent experiments.

Figure 6 Inactivation of *Myb* is an underlying cause for accumulation of IMLEC.

(**A**) Reduction of *Myb* mRNA in the *Rptor*-deficient HSPCs. BM LSK and CMP populations were FACS-sorted from Ctrl and cKO mice at 1-3 weeks after pIpC treatment. Quantitation of *Myb* mRNA was performed by qPCR. n=5 for Ctrl-LSK; n=4 for cKO-LSK (left). n=4 for Ctrl-CMP; n=3 for cKO-CMP (right). (**B**) Detection of c-Myb protein by intracellular staining. Data represent one of three independent experiments with similar results. (**C**-**E**) Deletion of c-Myb in mice

with homozygous floxed *Myb* resulted in enhanced generation of IMLECs. (**C**) Schematic of experimental design. Sex-matched 6-8 weeks old c-Myb Ctrl (*Myb* $^{F/F}$) and cKO (*Myb* $^{F/F}$*, Mx1-Cre*) mice were treated with pIpC for 7 times. The phenotypes were analyzed on day 7 after the complement of pIpC treatment. Inducible deletion of c-Myb showed obvious increase of PD-L1 expression on $CD11b^{+}Gr\text{-}1^{-}$ BM cells (**D**) and production of IMLECs (**E**). n=3 for c-Myb Ctrl mice; n=3 for c-Myb cKO mice. (**F-H**) Deletion of *Myb* enhances generation of IMLEC. (**F**) Diagram of experimental design. Whole BM cells ($2X10^6$/mice) of given genotypes were used for transplantation. Once the chimera mice were established, deletion of *Myb* was induced by five daily injection of tamoxifen. (**G**) Detection of *Myb* deletion in the whole BM cells after tamoxifen treatments. Data are representative of two independent experiments. (**H**) Generation of IMLEC is promoted by inactivation of *Myb.* BM cells were harvested at 7 days after first tamoxifen treatment and analyzed for IMLECs based on surface markers CD11b, Gr-1 and PD-L1 within the donor-derived $CD45.2^{+}$ BM cells. Data shown represent one of three experiments using either first or second generation of BM chimeras. (**I**) *Rptor* deletion broadly increases miRNAs targeting *Myb*. Lin^{-} $c\text{-}Kit^{+}$ HSPCs were isolated from Raptor Ctrl and cKO mice at 10 days after pIpC treatment. miRNA levels were measured by miRNA microarray. The y-axis shows the $\log_2$ ratio of signal, while the x-axis shows the $-\log_{10}P$ value. The doted boxes show the numbers of significantly ($P<0.05$) up-regulated (fold change>2) or down-regulated (fold change <0.5) miRNAs among 50 miRNAs with mirSVR

score < -1.0. Each dot represents the mean value of a unique miRNA from 3 independent samples.

Figure 7 IMLECs broadly express PPRs and produce large amounts of inflammatory cytokines upon stimulation by various TLR ligands.

(**A**) Heat map showing the relative transcript levels of TLRs among the indicated populations. (**B**) Both WT and Raptor-cKO IMLECs have greatly elevated expression of multiple TLRs genes in comparison to Ctrl BM. q-PCR was performed to determine transcript levels of *Tlr1-9* genes. After normalizing for cDNA input based on *Hprt* mRNA in each sample, the *Tlr1-9* levels in the FACS-sorted cKO $CD11b^+$ $Gr\text{-}1^-$ BM IMLEC were compared with Ctrl BM (artificially defined as 1.0). n=3 for Ctrl WBM; n=5 for cKO- IMLEC; n=5 for WT-IMLEC. Similar results were obtained using mice sacrificed at 2 weeks ~ 2 months after pIpC treatment. (**C, D**) In responses to various TLR ligands, *Rptor* cKO BM cells produced greatly elevated amounts of TNF-α (**C**) and MCP-1 (**D**) than the Ctrl BM. Data shown are from one experiment involving 3 repeats per group and have been reproduced in five independent experiments. (**E**) Lin^- ($B220^-CD3^-$ $Ter119^-Gr\text{-}1^-NK1.1^-F4/80^-CD115^-$) $CD11b^+$ $PD\text{-}L1^+$ IMLECs from both cKO and WT BM were robust TNF-α producers after stimulation with LPS. BM cells ($1X10^7$ cells / well) were stimulated with LPS (1μg/ml) for 16 hours with the presence of Golgi blocker in the last 4 hours. Data shown are representative profiles from one experiment and have been reproduced in 3 independent experiments.

Figure 8 Rptor cKO mice are hyper sensitive to challenges by TLR ligands. (**A**) High blood levels of inflammatory cytokines in cKO mice that have received 7 pIpC treatments. Serum samples collected at 7 days after the last pIpC treatment were tested for levels of IL-12p70, TNF-α, IFN-γ, MCP-1, IL-10 and IL-6. Dot plots depict cytokine levels in individual cKO (red dots) or Ctrl (blue dots) mice, and line drawings depict means and SD. n=12 for Ctrl mice and n=11 for cKO mice. (**B**) High proportions of *Rptor* cKO mice that received 7 pIpC injections died within 7 weeks after first pIpC treatment. Data shown are Kaplan-Meier survival curve, and the statistical significance is determined by log-rank test. n=32 for Ctrl mice and n=31 for cKO mice. (**C**) Representative H&E staining of liver sections from *Rptor* Ctrl and cKO mice at 2 weeks post pIpC treatment. Scale bars represent 200μm (10X) and 50μm (40X), respectively. (**D, E**) Massive accumulation of IMLEC in cKO liver. (**D**) Accumulation of $CD11b^{+}$ $Gr\text{-}1^{-}$ cells in the cKO liver. (**E**) $CD11b^{+}$ $Gr\text{-}1^{-}$ cells in cKO livers demonstrated IMLEC surface markers, including PD-$L1^{high}$ and $F4/80^{low/-}$. Gray lines indicate the staining for isotype control antibodies. Results are representative of at least five independent analyses. (**F-H**) cKO mice are vulnerable to low doses of LPS challenges. At 2-3 months after pIpC treatments, cKO and Ctrl mice were challenged with 5mg/kg body weight of LPS and observed survival. (**F**) Kaplan-Meier survival analysis. Data are pooled from 3 independent experiments. n=14 for Ctrl mice; n=11 for cKO mice. Inflammatory cytokines TNF-α (**G**) and MCP-1 (**H**) levels from mice serum before (0h) and at 6 hours after (6h) LPS injection are

shown. n=10 for Ctrl mice; n=9 for cKO mice. Note greater than 500-fold increase in plasma TNF-α levels. (**I**, **J**) cKO mice mounted enhanced inflammatory response to acetaminophen-triggered liver necrosis. Serum TNF-α (**I**) and MCP-1(**J**) levels at 6 hours upon acetaminophen (3.2 mg/mouse) treatment are shown. n=4 for Ctrl mice; n=6 for cKO mice. Mann-Whitney test was used for statistics analysis, and lines indicate Mean ±SD. Similar trends were observed in another independent experiment.

Figure 9 *Rptor* deletion in hematopoietic cells greatly increased vulnerability of mice to pIpC.

(**A**) Diagram of experimental design. WT CD45.1^{+} recipient mice were irradiated and transplanted with 5X10^{6} BM cells from *Rptor*$^{F/F}$ and *Rptor*$^{F/F}$*, Mx1-Cre* BM. After the fully reconstitution, recipients were treated with pIpC 3 times every other day to induce gene deletion in chimera mice with cKO BM. 10 days after the last injection of pIpC, recipients were challenged with another pIpC injection and the survival of mice were followed for 4 more weeks. Arrows denote the injections of pIpC at indicated time points. (**B**) Kaplan-Meier survival analysis after pIpC treatments. n= 12 for Ctrl chimera mice; n=15 for cKO chimera mice. (**C**) Histological analysis of liver sections after H&E staining. Note extensive inflammation and liver damage in cKO chimera mice. Scale bars represent 200μm (10X), 100μm (20X) and 50μm (40X). (**D-F**) Identification of IMLEC in BM (**D**), spleen (**E**) and livers (**F**) by flow cytometry. Mice were euthanized 45 days after the first pIpC injection. The distinct CD11b^{+} Gr-1^{-} PD-L1^{+} F4/80$^{low/-}$ IMLECs

greatly enriched in BM, spleen and liver of recipients of *Rptor* cKO BM. FACS profiles shown represent one of five independent experiments.

Figure Supplements and Supplementary Files

Figure 1—figure supplement 1 Conditional deletion of *Rptor* resulted in abnormal hematopoiesis.

(**A**) Deletion of *Rptor* in BM cells. PCR were performed to check the deletion in BM from mice 2 weeks after pIpC treatment (for Ctrl and cKO mice, no treatment for WT mice). (**B**) Representative pictures of leg bones (tibiae and femurs), spleen, and thymus harvested from mice on day 30 post pIpC treatment. (**C**) Histology findings in the cKO spleen by H&E staining. Up left panel: a spleen histological section showing expanded white pulp areas (WP) and compressed intervening red pulp (RP). The white pulp contains an increased population of lightly staining cells that sometimes is situated in the marginal zones and follicular centers (B cell areas) and sometimes infiltrates the periarteriolar sheaths (T cell area, long arrow). Up right panel: normal splenic architecture from control mouse. Scale bar, 200 μm. Down left panel: higher magnification of expanded cell population within the splenic white pulp. Morphologically these cells resemble germinal center lymphocytes. There are both smaller cells with cleaved nuclei (long arrow) resembling centrocytes and larger cells with 1-2 prominent nucleoli resembling centroblasts (short arrow). There are small

numbers of plasmacytoid cells (arrowhead). Down right panel: histological section of splenic red pulp Red pulp of the spleen showing foci of extramedullary hematopoiesis with decreased erythroid (short arrow) and myeloid (long arrow) progenitors. The erythroid lineage contains occasional foci of pyknotic or karyorrhectic (fragmented) nuclei consistent with cell death (asterisk). Scale bar, 20 μm. (**D**) The cellularities of splenocytes (left) and thymocytes (right) from mice at day 30 post pIpC treatment. n=6 for Ctrl mice; n=5 for cKO mice. (**E**) BM cellularities (left) and spleen/body weight ratios (right) for mice on day 7 and day 30 after pIpC treatment. n=3~8 for Ctrl mice; n=5~6 for cKO mice.

Figure 1—figure supplement 2 Raptor deletion led to impaired developments of B lymphoid, erythroid and myeloid compartments in BM. (**A**) Representative FACS profiles for Pro B ($CD127^+B220^+BP\text{-}1^-IgM^-IgD^-$ cells), Pre B ($CD127^+B220^+BP\text{-}1^+IgM^-IgD^-$ cells), Immature B ($CD127^-B220^+BP\text{-}1^-IgM^+IgD^-$ cells), Mature B ($CD127^-B220^+BP\text{-}1^-IgM^+IgD^+$ cells) in mice BM on day 7 after pIpC treatment. (**B**) Frequencies of BM B cells subsets as in (A). n=5 for Ctrl mice and n=6 for cKO mice. (**C**) Representative FACS analysis of erythroid populations in BM by Ter119 and CD71. Roman numerals and numbers indicate the identity and percentages of the developmentally defined subpopulations: I, proerythroblasts; II, basophilic erythroblasts; III, polychromatophilic erythroblasts; IV, orthochromatophilic erythroblasts. (**D**) Frequencies of erythroblast subsets in mice BM. n=5 for Ctrl mice and n=6 for cKO mice. (**E**, **F**) Size and granularity of BM $CD11b^+$ $Gr\text{-}1^-$ IMLECs from *Rptor* cKO mice. (**E**) Flow cytometric assays for

size and granularity of Ctrl and cKO BM cells by FSC and SSC, respectively. Erythroid cells with smaller size and granularity were excluded in the initial gating. DP (double positive) represents $CD11b^+$ $Gr\text{-}1^+$ granulocytes, and DN (double negative) represents ($CD11b^-$ $Gr\text{-}1^-$) cells. (**F**) Relative size (FSC-A) and granularities (SSC-A) of DN, DP and IMLEC. The mean values in Ctrl mice are artificially defined as 100%. n=5 for Ctrl mice; n=3 for cKO mice.

Figure 1—figure supplement 3 *Rptor* cKO mice are pancytopenic.

(**A**) Complete blood cell counts (CBC) data for Ctrl and cKO mice on day 30 after pIpC treatment. WBC, white blood cells; NE, neutrophils; LY, lymphocytes; MO, monocytes; RBC, red blood cells; Hb, hemoglobin; PLT, platelets. Means of the Ctrl mice in each experiment are artificially defined as 100%. (**B**) Representative FACS profiles showing the percentages of different leukocyte populations in peripheral blood from Ctrl and cKO mice on day 30 after pIpC treatment. (**C, D**) Reduction of leukocyte populations in the peripheral blood of cKO mice. Frequencies among $CD45.2^+$ leukocytes (**C**) and absolute numbers (**D**) of various cell types in blood on day 30 after pIpC treatment are shown. n=7 for Ctrl mice; n=6 for cKO mice. Data represent one of three independent experiments with similar results.

Figure 1—figure supplement 4 *Rptor* deletion increased hematopoietic stem and progenitor cells in BM.

(**A**) Representative FACS profiles for Lin^- $Sca\text{-}1^+$ $c\text{-}Kit^+$ cells (LSK, identified as $CD3^-$ $B220^-$ $Ter119^-$ $CD11b^-$ $Gr\text{-}1^-$ $Sca\text{-}1^+$ $c\text{-}Kit^+$ cells), multipotent progenitor cells (MPP, identified as Lin^- $Sca\text{-}1^+$ $c\text{-}Kit^+$ $CD150^-$ $CD48^+$ cells), short-term HSC (ST-HSC, identified as Lin^- $Sca\text{-}1^+$ $c\text{-}Kit^+$ $CD150^+$ $CD48^+$ cells) and long-term HSC (LT-HSC, identified as Lin^- $Sca\text{-}1^+$ $c\text{-}Kit^+$ $CD150^+$ $CD48^-$ cells) in the BM from Raptor Ctrl and cKO mice on day 7 after pIpC treatment. Numbers indicate the percentages of gated populations in total BM cells. (**B**) Frequencies (left) and absolute numbers (right) of stem and progenitor cells as in (A) are shown. n=6 for Ctrl mice; n=7 for cKO mice. (**C**) Representative FACS profiles for common myeloid progenitor (CMP, identified as Lin^- $Sca\text{-}1^-$ $c\text{-}Kit^+$ $CD34^{Medium}CD16/32^{Medium}$ cell), granulocyte / macrophage progenitor (GMP, identified as Lin^- $Sca\text{-}1^-$ $c\text{-}Kit^+$ $CD34^+$ $CD16/32^+$ cell) and megakaryocyte / erythroid progenitor (MEP, identified as Lin^- $Sca\text{-}1^-$ $c\text{-}Kit^+$ $CD34^-$ $CD16/32^-$ cell) in BM. (**D**) Frequencies (left) and absolute numbers (right) of myeloid progenitors as in (C) are shown. n=5 for Ctrl mice; n=5 for cKO mice.

Figure 1—figure supplement 5 Tamoxifen induced conditional deletion of *Rptor* in hematopoiesis also led to massive accumulation of IMLECs.

(**A**) Schematic of experimental design. Sex-matched 6-8 weeks old Ctrl (*Rptor* $^{F/F}$) and cKO (*Rptor* $^{F/F}$, *CreER*) mice were treated with Tamoxifen for 5 consecutive days. The phenotypes were analyzed 3 weeks after the first treatment. (**B**) Representative flow cytometric analysis of myeloid cells from Ctrl and cKO mice BM by CD11b, Gr-1 and PD-L1. (**C**) *Rptor* deletion caused expansion of Lin^-

(B220$^-$ CD3$^-$ Ter119$^-$ NK1.1$^-$ Gr-1$^-$ F4/80$^-$ CD115$^-$) CD11b$^+$ PD-L1$^+$ IMLECs in BM. (**D**) Schematic of experimental design. CD45.2$^+$ Ctrl BM and cKO BM were transplanted into lethal dose irradiated CD45.1$^+$ recipient mice. Tamoxifen treatment of recipient mice was started 6 weeks after fully reconstitution of donor-derived cells. The phenotypes were analyzed 3 weeks after the first treatment. (**E**, **F**) Representative flow cytometrical profiles of donor-derived CD45.2$^+$ Myeloid cells (**E**) and IMLECs (**F**) in BM of recipient mice are shown as in (B) and (C), respectively.

Figure 2—figure supplement 1 *In silico* pair wise comparisons between IMLECs and other closely related leukocytes based on our RNA-seq data and the publically available RNA-seq data.

(**A**-**D**)Based on the space proximity in the PCA data, macrophage (**A**), B precursor (**B**), naive B (**C**) and granulocyte (**D**) were selected for one-to-one comparison. Numbers in corners indicate amounts of genes significantly (FDR-adjusted p-value<0.05) up-regulated (right) or down-regulated (left) by at least 4-fold. (**E**, **F**) IMLECs in Raptor cKO BM are distinct from all DC subsets tested. (**E**) Principal component analysis (PCA) of gene expression in Raptor cKO CD11b$^+$ Gr-1$^-$ BM cell (IMLEC), macrophage, B precursors and various *ex vivo* DC subsets. Numbers along axes indicate relative scaling of the principal variables. (**F**) Clustering of IMLEC, macrophage, B precursors with other DC subsets based on their gene expression profiles. Hierarchical clustering with complete linkage was carried out using the R software. The public RNA-seq datasets for DC

subsets used are as followings: CDP (common DC precursor, GSM1531794); pDC (GSM1531795); preDC (GSM1531796); DN DC (CD4 and CD8 double negative DC, GSM1531797); $CD4^+$ DC (GSM1531798) and $CD8^+$ DC (GSM1531799).

Figure 2—figure supplement 2 cKO IMLECs have a similar expression patterns as that of B-lymphoid subsets in the sterile transcripts from *Igk* and *Igl* loci.

(**A, B**) Genome browser display of transcript expression of *Igk* locus in chromosome 6 (**A**) and *Igl* locus in chromosome 16 (**B**). For each track, the y-axis is the normalized number of aligned reads counts of gene region, whereas the x-axis depicts physical distance in base-pairs (bp). Numbers on top indicate the start and end positions of specified gene regions.

Figure 4—figure supplement 1 Comparisons of surface markers, viability and cellular proliferation among IMLECs and other defined lineages.

(**A**) IMLECs from Raptor Ctrl and cKO BM displayed comparable expression levels of MHC-I, MHC-II and other surface markers (Ly6C, CD14 and CD68). Data shown are representative of 3 independent experiments. (**B, C**) IMLECs from Raptor Ctrl and cKO BM exhibited much slower proliferation than other BM lineages. Representative flow profile (**B**) and summary data (**C**) are from BrdU incorporation assays. (**D**, **E**) IMLECs from Raptor Ctrl and cKO BM were more prone to apoptosis than other BM lineages. Representative flow profile (**D**) and

summary data (**E**) are from Annexin V and 7-AAD staining. B cells, $B220^+$ BM cells; T cells, $CD3^+$ BM cells; Granulocytes, $CD11b^+Gr\text{-}1^+$ BM cells. n=5 for Ctrl mice; n=5 for cKO mice.

Figure 6—figure supplement 1 c-Myb expression and accumulation of IMLECs. (**A**-**C**) Induced deletion of c-Myb in mice with heterozygous floxed c-Myb (*Myb* $^{F/+}$*, Mx1-Cre*) did not show significant accumulation of IMLECS in mouse BM. (**A**) Schematic of experimental design. Sex-matched 6-8 weeks old Ctrl (*Myb* $^{F/+}$) and heterozygous floxed c-Myb (*Myb* $^{F/+}$*, Mx1-Cre*) mice were treated with pIpC for 7 times. The phenotypes were analyzed on day 7 after the complement of pIpC treatment. (**B**) Representative flow profile of BM IMLECs. (**C**) Detection of *Myb* deletion in the whole BM cells after pIpC treatment. Data in (B) and (C) are representative results of independent experiments with 3 groups of paired mice. (**D**-**G**)The provision of heterologous c-Myb significantly diminished the generation of IMLECs from Raptor-deficient LSK cells. (**D**, **E**) *Myb*-expression lenti-virus (pWPI-Myb) was validated by intracellular staining (**D**) and western blot (**E**) of CHO cells 36 hours after virus infection. Lenti-virus with GFP co-expression (pWPI) was used as control. AF568, Alexa Fluor 568 dye. (**F**) Diagram of experimental design. $1X10^4$ LSK cells sorted from pIpC treated Raptor cKO mice were infected with indicated lenti-virus and subsequently co-cultured with the OP9 cells for 12 days. (**G**) GFP^+ cells with heterologous c-Myb expression did not give rise to $CD11b^+$ $Gr\text{-}1^-$ $PD\text{-}L1^+$ IMLECs. Data represent the results of two independent experiments.

Figure 7—figure supplement 1 IMLECs broadly over-express multiple families of pattern recognition receptors (PRRs) when compared with other blood cells.

(**A**) Heat map showing the relative expression levels of genes encoding key PRRs. TLRs, Toll-like receptors; NLR, Nod-like receptors; RLRs, RIG-I-like receptors; ALRs, Aim2-like receptors. (**B**) mRNA levels of the indicated PPRs genes were measured by q-PCR in WBM cells from Ctrl mice and $CD11b^{+}$ $Gr\text{-}1^{-}$ BM IMLECs from cKO mice. n=3 for Ctrl WBM; n=5 for cKO BM IMLECs.

Supplementary file 1 Transcript levels of CD markers analyzed from RNA-seq datasets. The FPKM values of 3 mice samples for cKO-IMLEC group (*Rptor* cKO $CD11b^{+}Gr\text{-}1^{-}$ BM IMLECs) and Ctrl-WBM group (Ctrl whole BM cells) are shown. Fold change indicates the ratio of average FPKM values.

Supplementary file 2 Expression levels of miRNAs targeting *Myb* in Raptor Ctrl and cKO BM HSPCs. The normalized signal values of 3 mice samples for cKO-HSPCs group and Ctrl-HSPCs group are shown. The microarray data have been deposited to NCBI GEO database with accession number GSE64042 as previously reported[43].

Supplementary file 3 The list of antibodies used for flow cytometry.

Supplementary file 4 Sequences of DNA primers used in PCR assays.

Figure 1

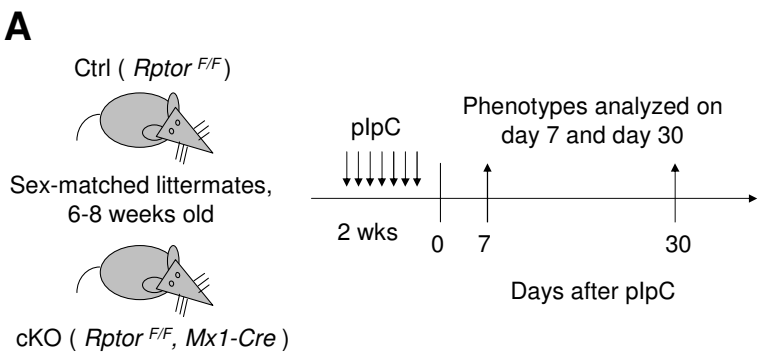
A
Ctrl (Rptor F/F)
Sex-matched littermates,
6-8 weeks old
cKO (Rptor F/F, Mx1-Cre)
pIpC
2 wks
0
7
30
Phenotypes analyzed on
day 7 and day 30
Days after pIpC

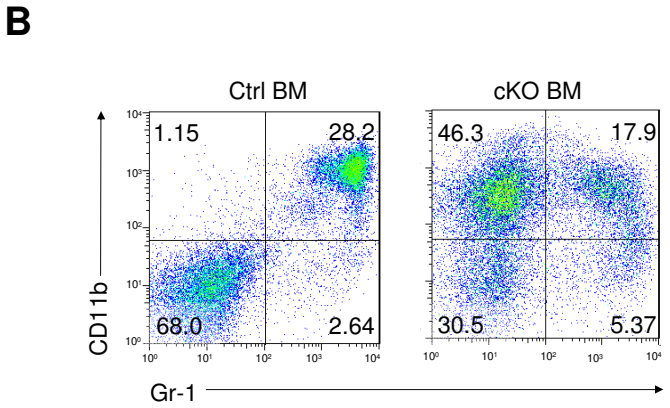
B
Ctrl BM
cKO BM
1.15
28.2
68.0
2.64
46.3
17.9
30.5
5.37
CD11b
Gr-1

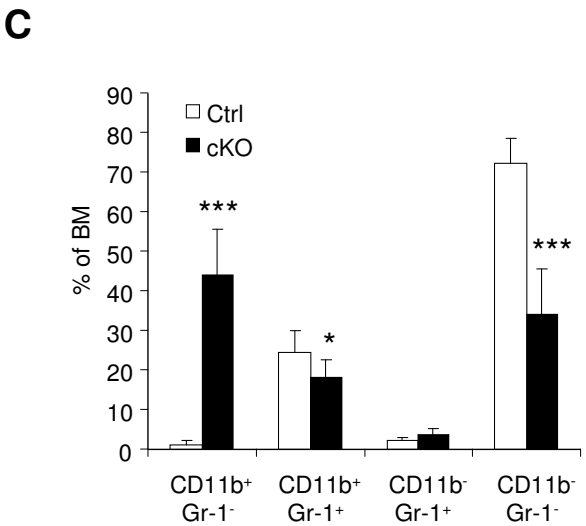
C
Ctrl
cKO
% of BM
***
*
***
CD11b+ Gr-1-
CD11b+ Gr-1+
CD11b- Gr-1+
CD11b- Gr-1-

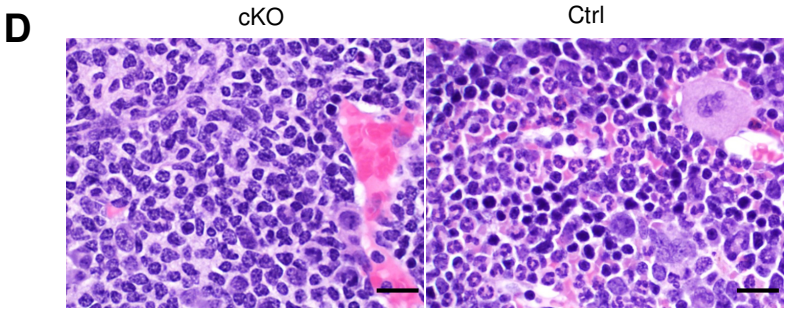
D
cKO
Ctrl

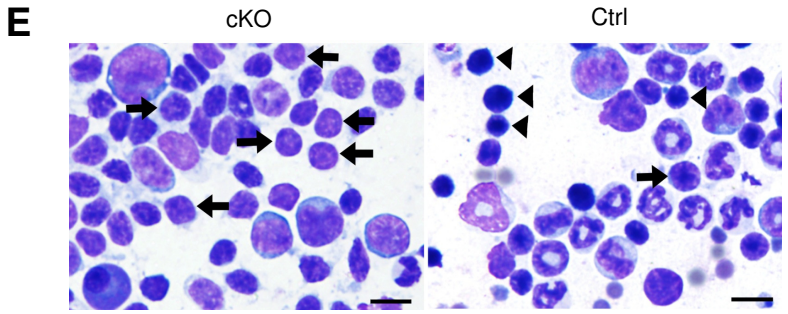
E
cKO
Ctrl

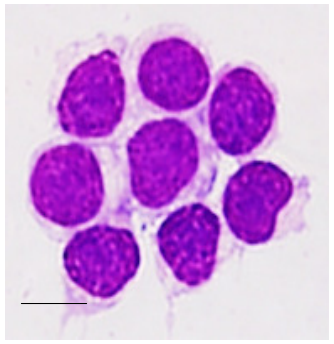
F

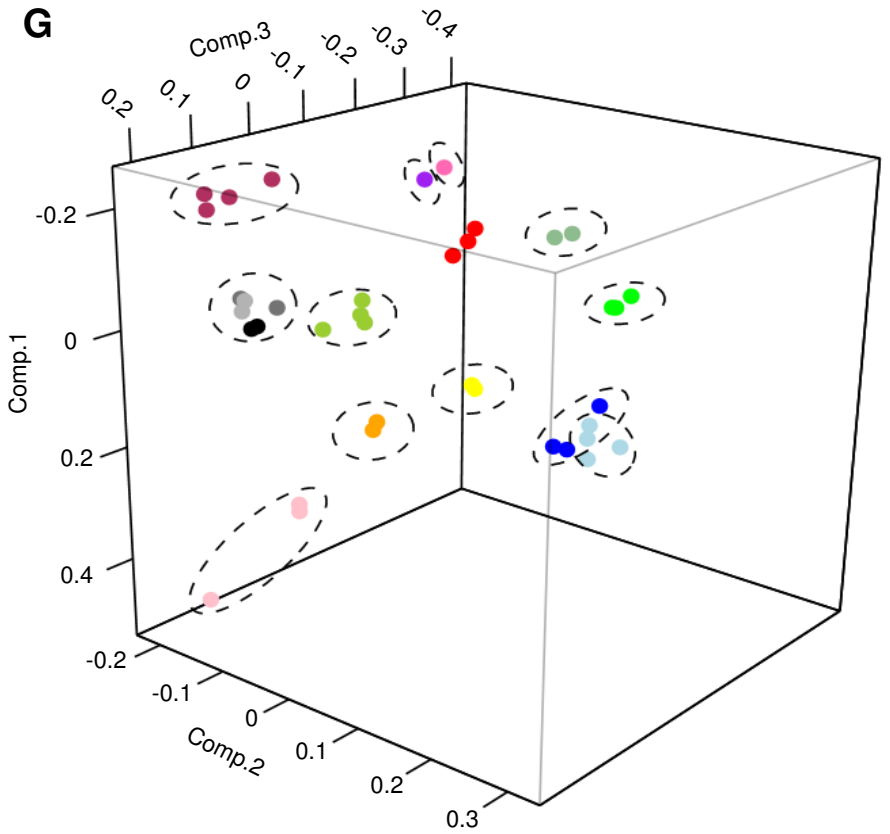
G
Comp.3
Comp.1
Comp.2
IMLEC
Pro-B
Pre-B
Naïve B
CD4 T
CD8 T
Treg
NK
Macrophage
Dendritic cell
Granulocyte
Neutrophil
Eosinophil
Basophil
Erythrocyte

Figure 1—figure supplement 1

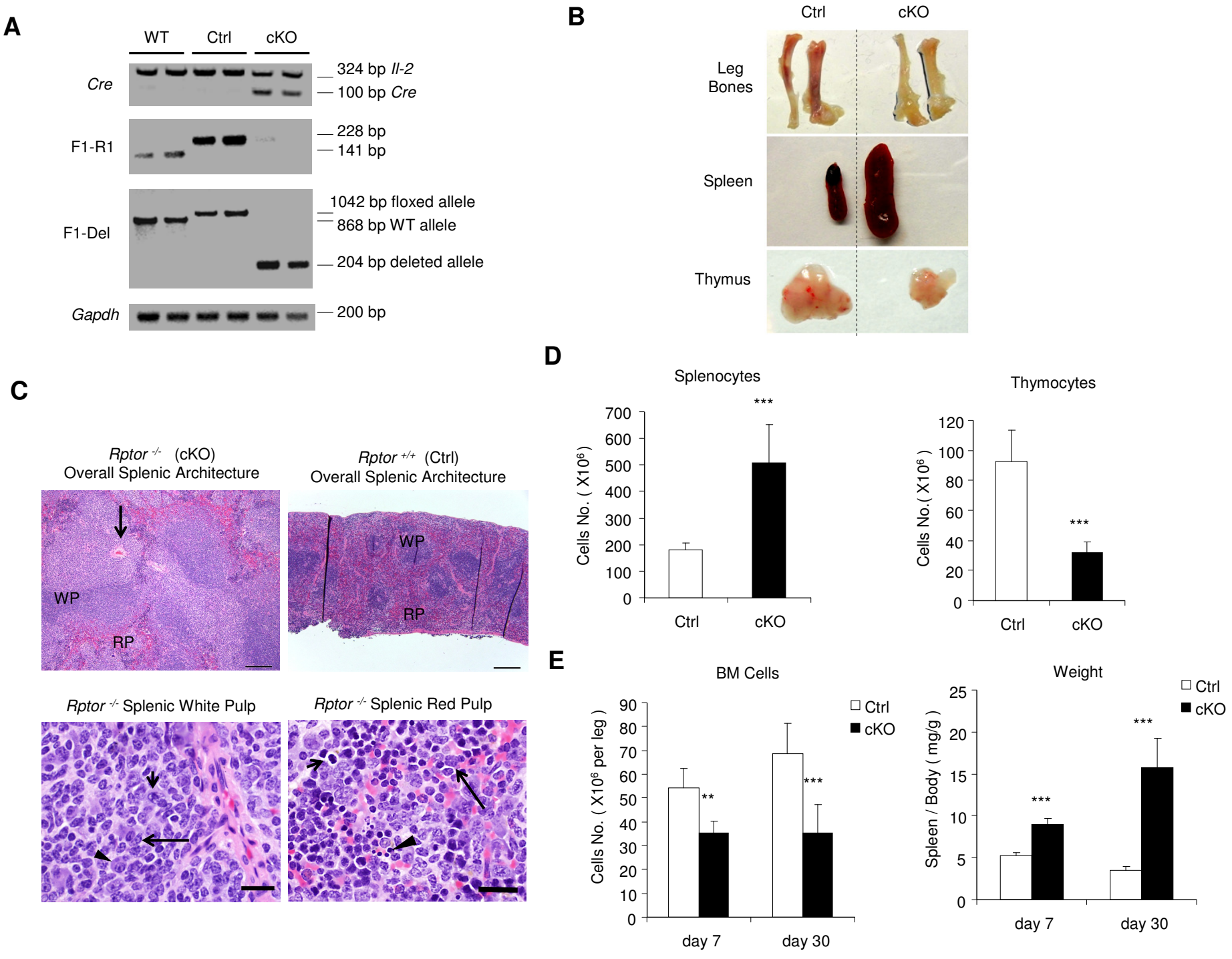

Figure 1—figure supplement 2

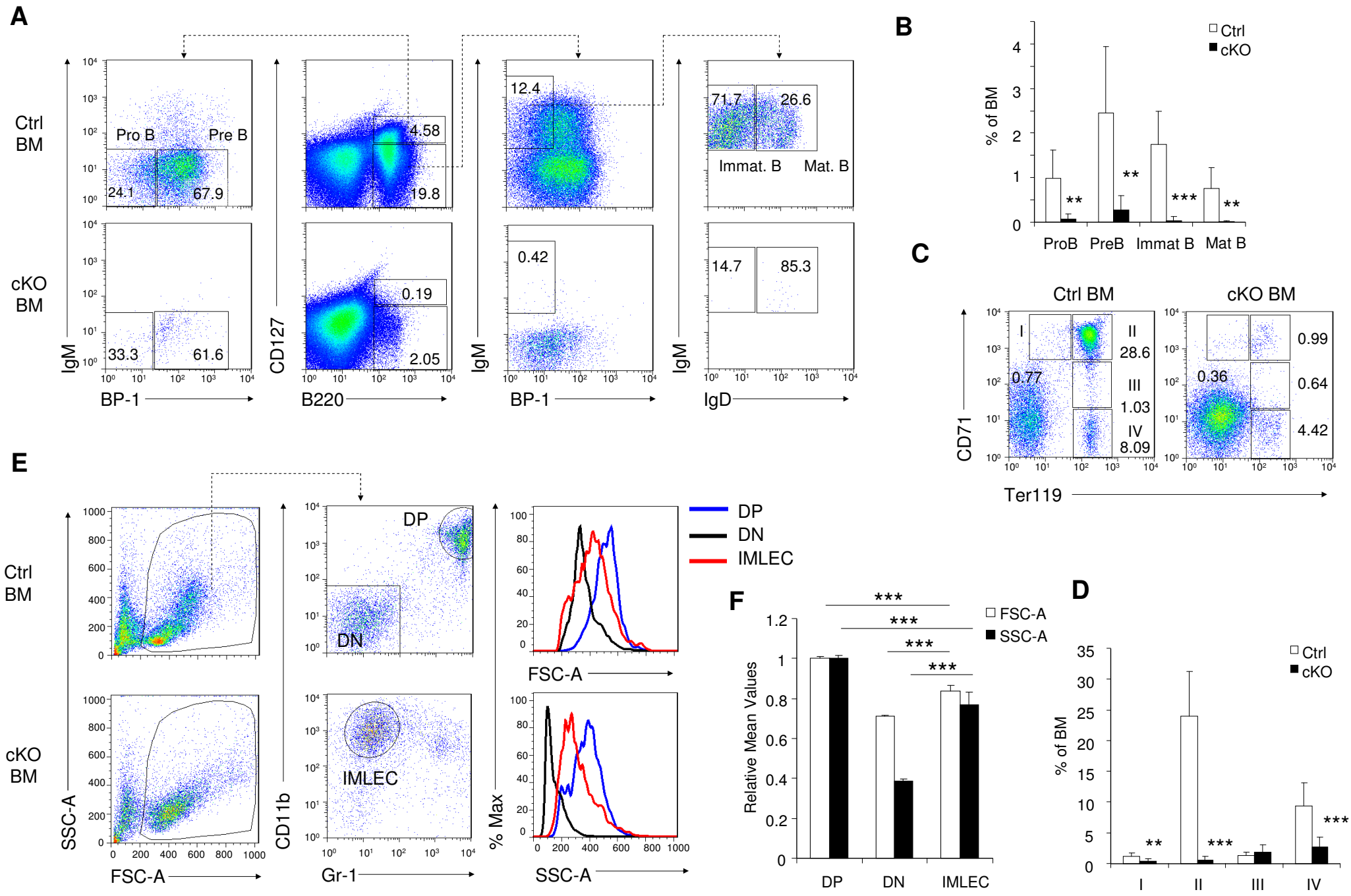

Figure 1—figure supplement 3

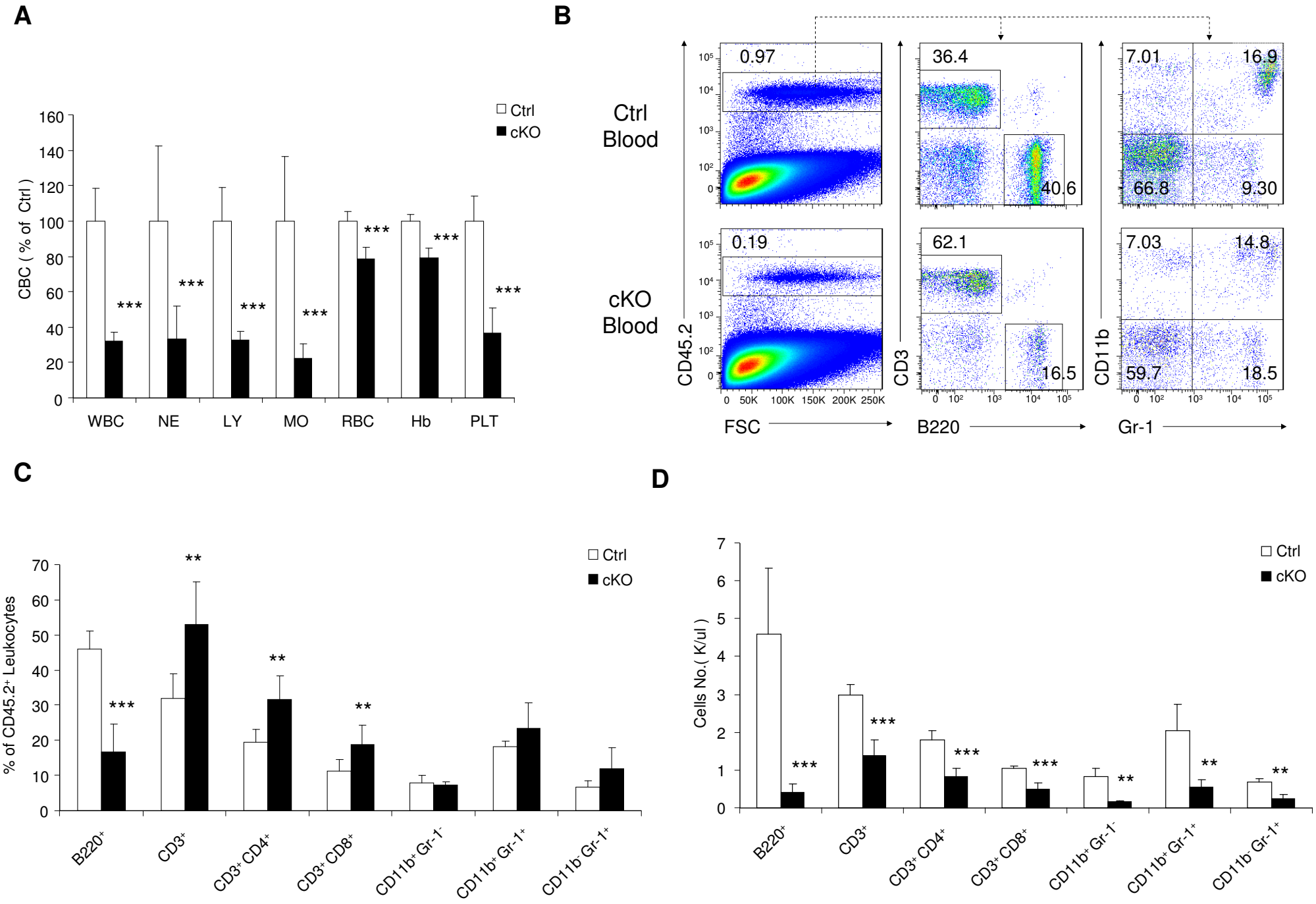

Figure 1—figure supplement 4

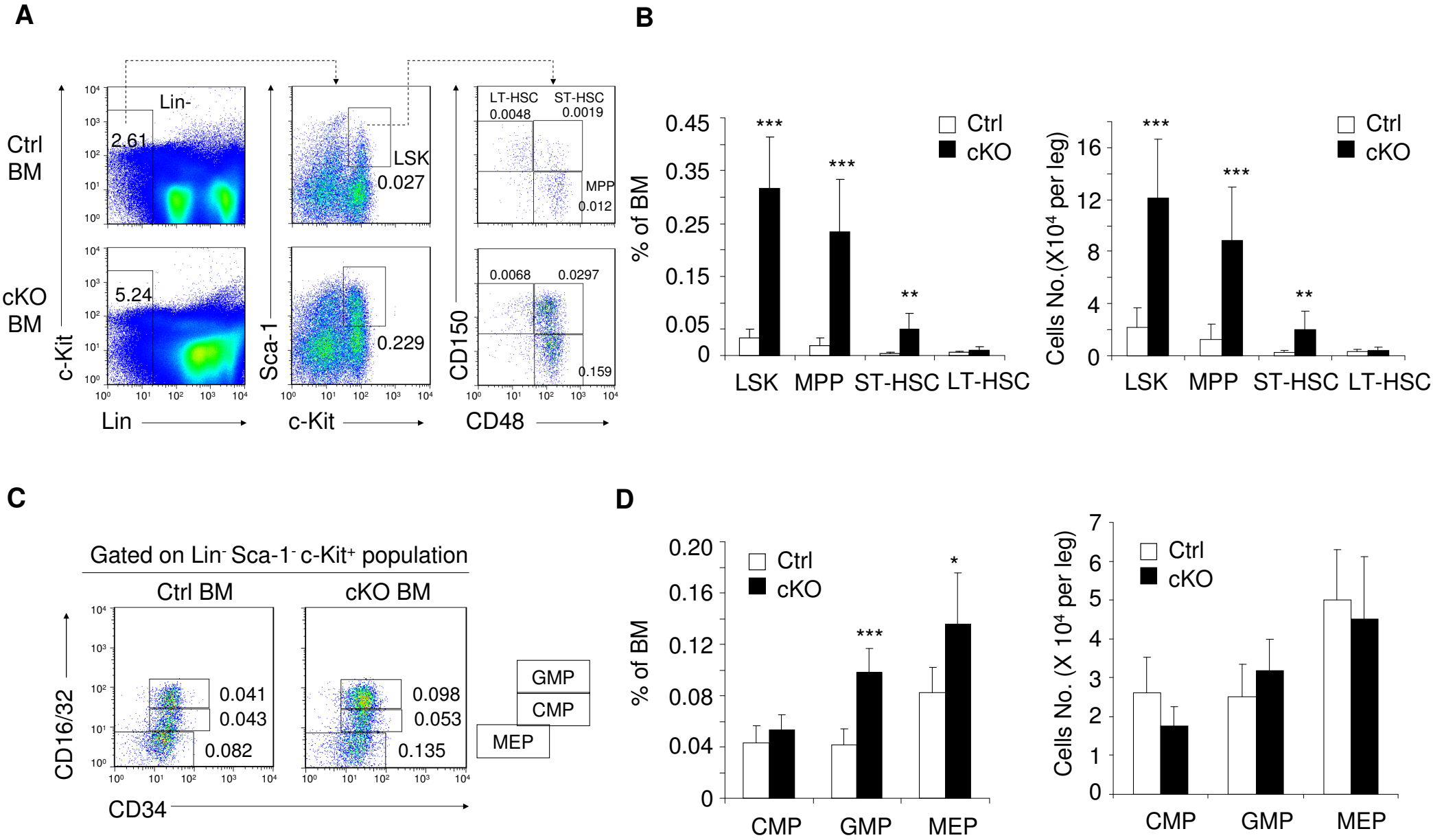

Figure 1—figure supplement 5

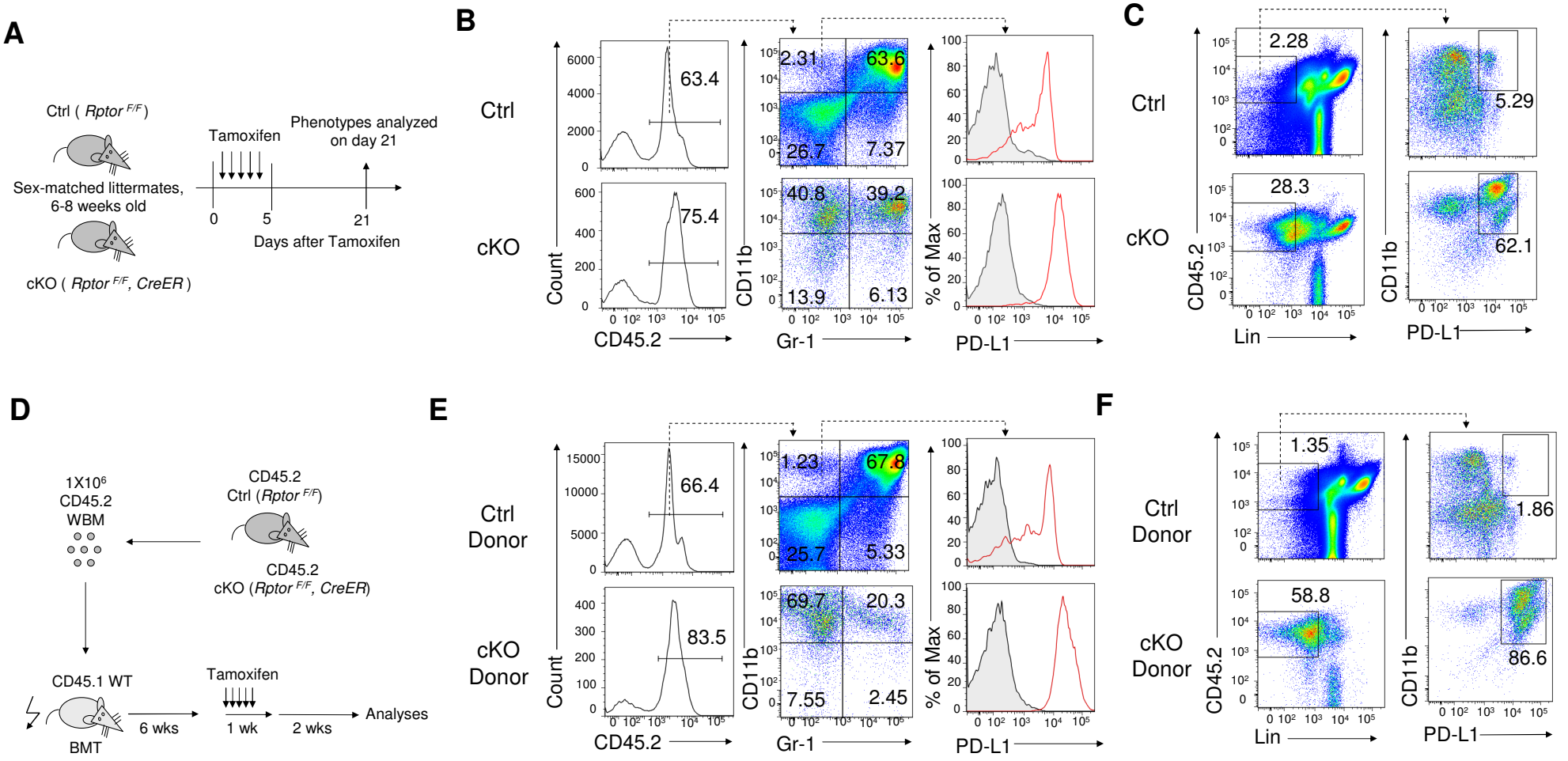

Figure 2

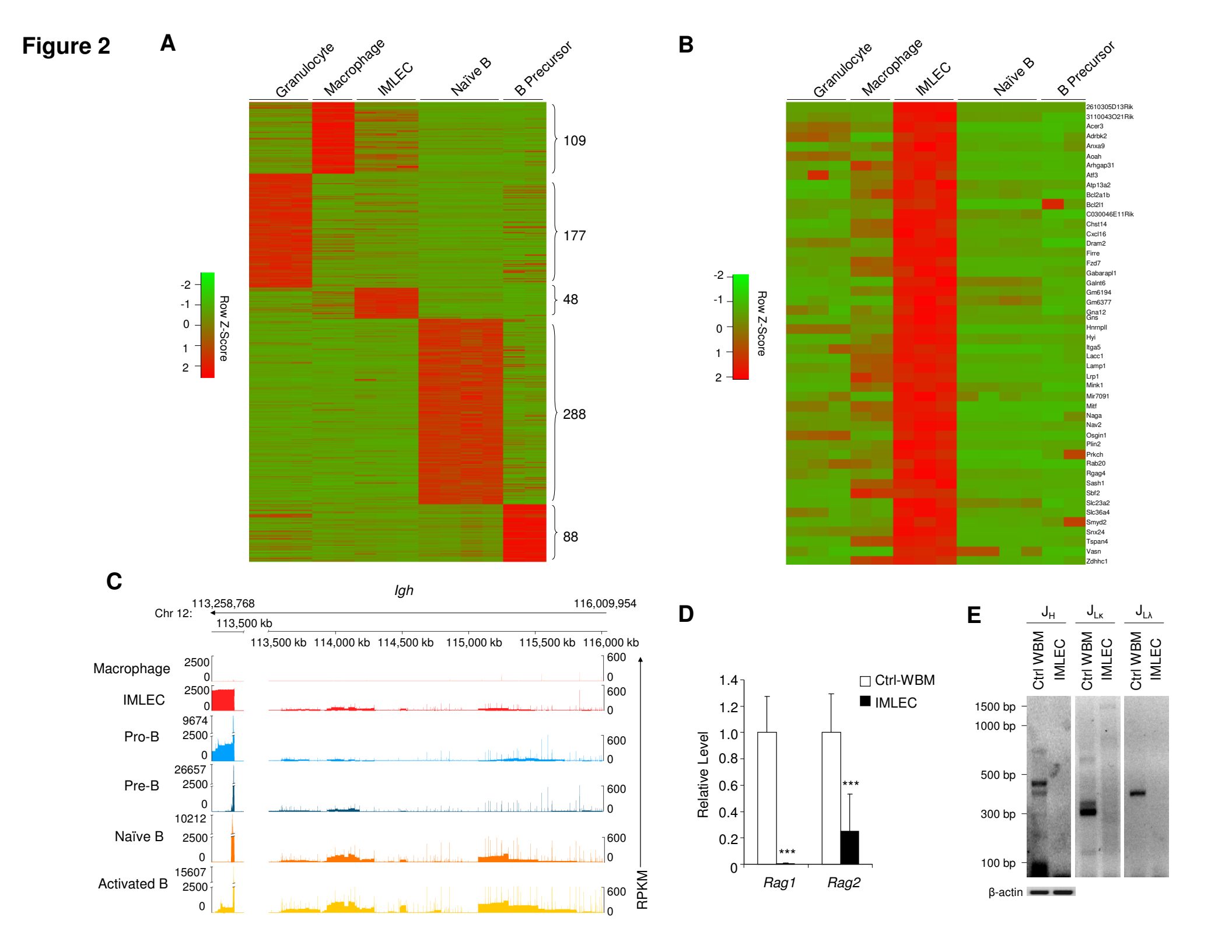
A
Granulocyte
Macrophage
IMLEC
Naïve B
B Precursor
109
177
48
288
88
Row Z-Score
-2
-1
0
1
2
B
Granulocyte
Macrophage
IMLEC
Naïve B
B Precursor
2610305D13Rik
3110043O21Rik
Acer3
Adrbk2
Anxa9
Aoah
Arhgap31
Atf3
Atp13a2
Bcl2a1b
Bcl2l1
C030046E11Rik
Chst14
Cxcl16
Dram2
Firre
Fzd7
Gabarapl1
Galnt6
Gm6194
Gm6377
Gna12
Gns
Hnrnpll
Hyi
Itga5
Lacc1
Lamp1
Lrp1
Mink1
Mir7091
Mitf
Naga
Nav2
Osgin1
Plin2
Prkch
Rab20
Rgag4
Sash1
Sbf2
Slc23a2
Slc36a4
Smyd2
Snx24
Tspan4
Vasn
Zdhhc1
Row Z-Score
C
Igh
Chr 12:
113,258,768
116,009,954
113,500 kb
113,500 kb
114,000 kb
114,500 kb
115,000 kb
115,500 kb
116,000 kb
Macrophage
IMLEC
Pro-B
Pre-B
Naïve B
Activated B
RPKM
D
Ctrl-WBM
IMLEC
Relative Level
Rag1
Rag2
***
E
J_H
J_Lκ
J_Lλ
Ctrl WBM
IMLEC
1500 bp
1000 bp
500 bp
300 bp
100 bp
β-actin

Figure 2—figure supplement 1

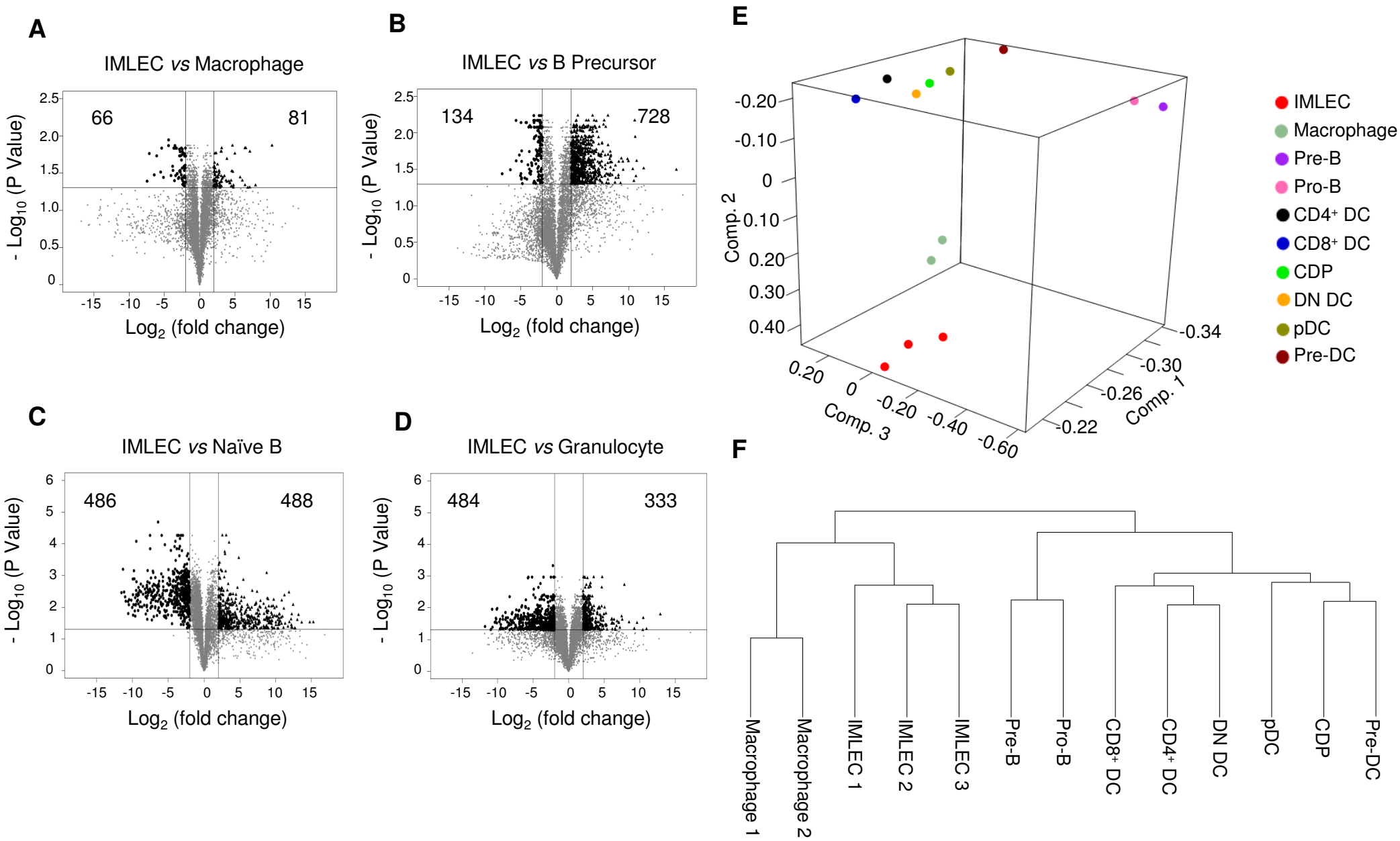

Figure 2—figure supplement 2

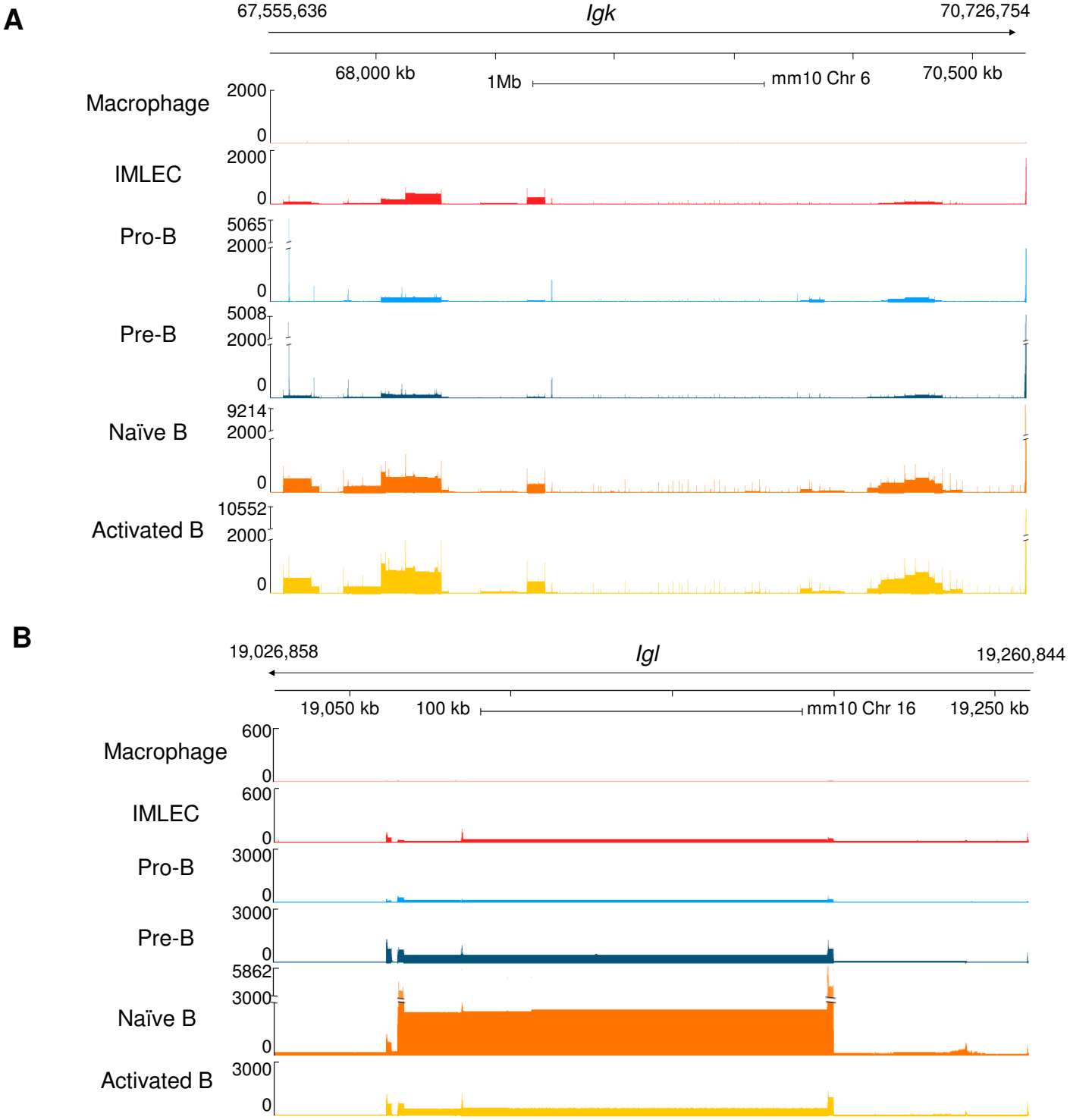

Figure 3

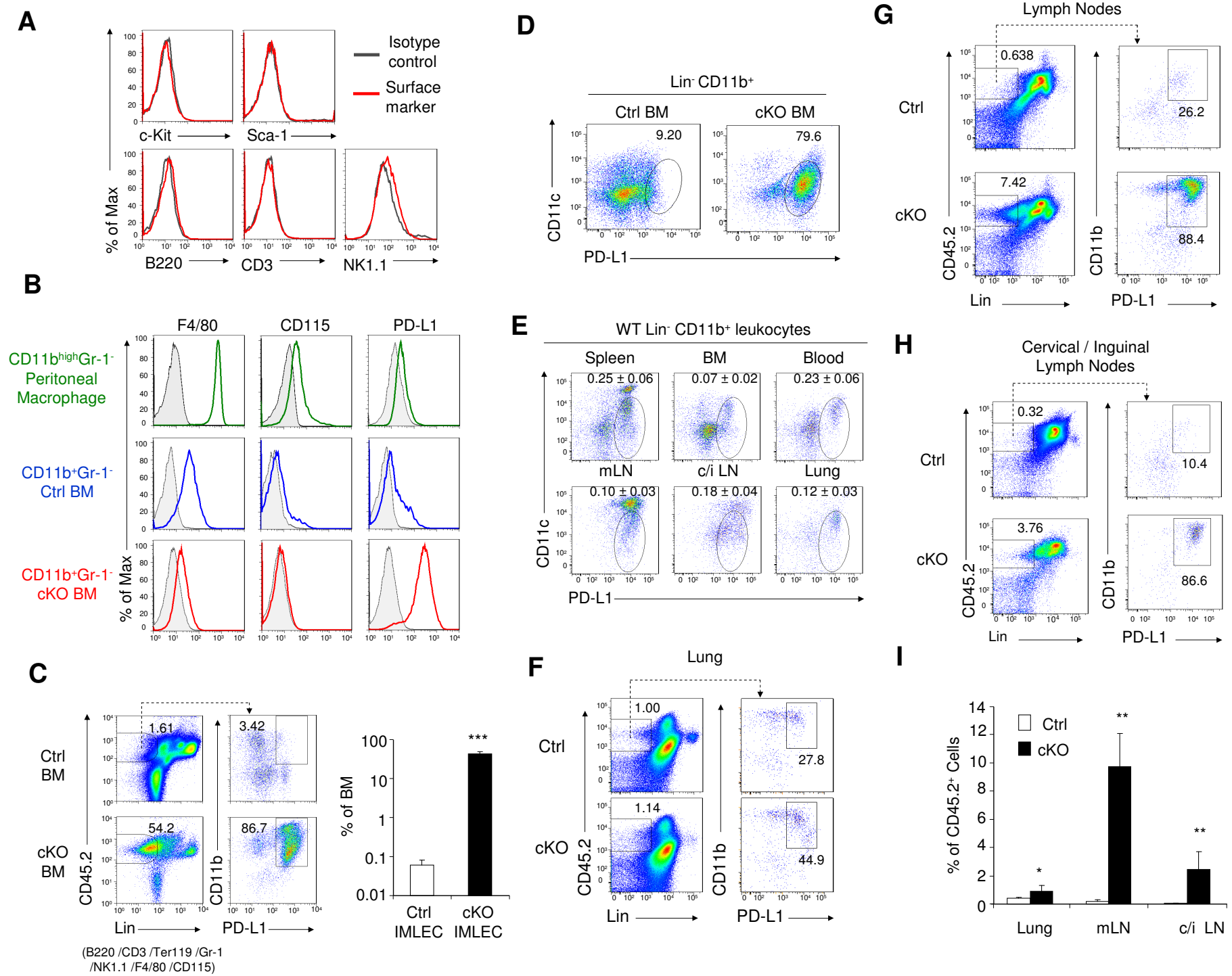
A
Isotype control
Surface marker
c-Kit
Sca-1
B220
CD3
NK1.1
% of Max
B
F4/80
CD115
PD-L1
CD11b^high Gr-1^- Peritoneal Macrophage
CD11b^+ Gr-1^- Ctrl BM
CD11b^+ Gr-1^- cKO BM
% of Max
C
Ctrl BM
cKO BM
1.61
3.42
54.2
86.7
CD45.2
CD11b
Lin
PD-L1
(B220 /CD3 /Ter119 /Gr-1 /NK1.1 /F4/80 /CD115)
% of BM
***
Ctrl IMLEC
cKO IMLEC
D
Lin- CD11b+
Ctrl BM
cKO BM
9.20
79.6
CD11c
PD-L1
E
WT Lin- CD11b+ leukocytes
Spleen
BM
Blood
0.25 ± 0.06
0.07 ± 0.02
0.23 ± 0.06
mLN
c/i LN
Lung
0.10 ± 0.03
0.18 ± 0.04
0.12 ± 0.03
CD11c
PD-L1
F
Lung
Ctrl
cKO
1.00
27.8
1.14
44.9
CD45.2
CD11b
Lin
PD-L1
G
Mesenteric Lymph Nodes
Ctrl
cKO
0.638
26.2
7.42
88.4
CD45.2
CD11b
Lin
PD-L1
H
Cervical / Inguinal Lymph Nodes
Ctrl
cKO
0.32
10.4
3.76
86.6
CD45.2
CD11b
Lin
PD-L1
I
Ctrl
cKO
% of CD45.2+ Cells
*
**
**
Lung
mLN
c/i LN

Figure 4

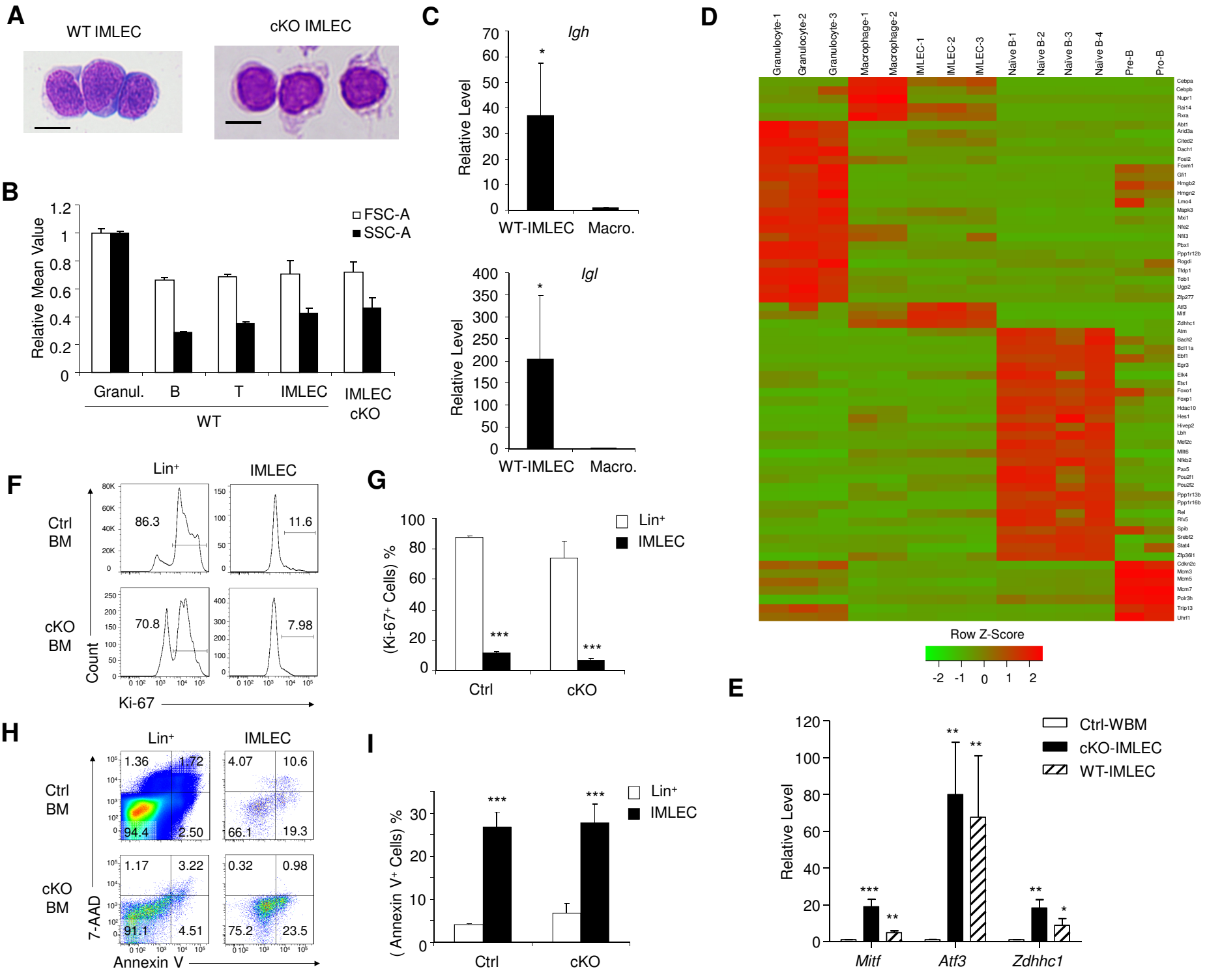
A
WT IMLEC
cKO IMLEC
B
Relative Mean Value
FSC-A
SSC-A
Granul.
B
T
IMLEC
IMLEC cKO
WT
C
Igh
Igl
Relative Level
WT-IMLEC
Macro.
D
Granulocyte-1
Granulocyte-2
Granulocyte-3
Macrophage-1
Macrophage-2
IMLEC-1
IMLEC-2
IMLEC-3
Naïve B-1
Naïve B-2
Naïve B-3
Naïve B-4
Pre-B
Pro-B
Row Z-Score
E
Ctrl-WBM
cKO-IMLEC
WT-IMLEC
Mitf
Atf3
Zdhhc1
F
Lin+
IMLEC
Ctrl BM
cKO BM
Count
Ki-67
86.3
11.6
70.8
7.98
G
(Ki-67+ Cells) %
Ctrl
cKO
H
7-AAD
Annexin V
1.36
1.72
94.4
2.50
4.07
10.6
66.1
19.3
1.17
3.22
91.1
4.51
0.32
0.98
75.2
23.5
I
(Annexin V+ Cells) %

Figure 4—figure supplement 1

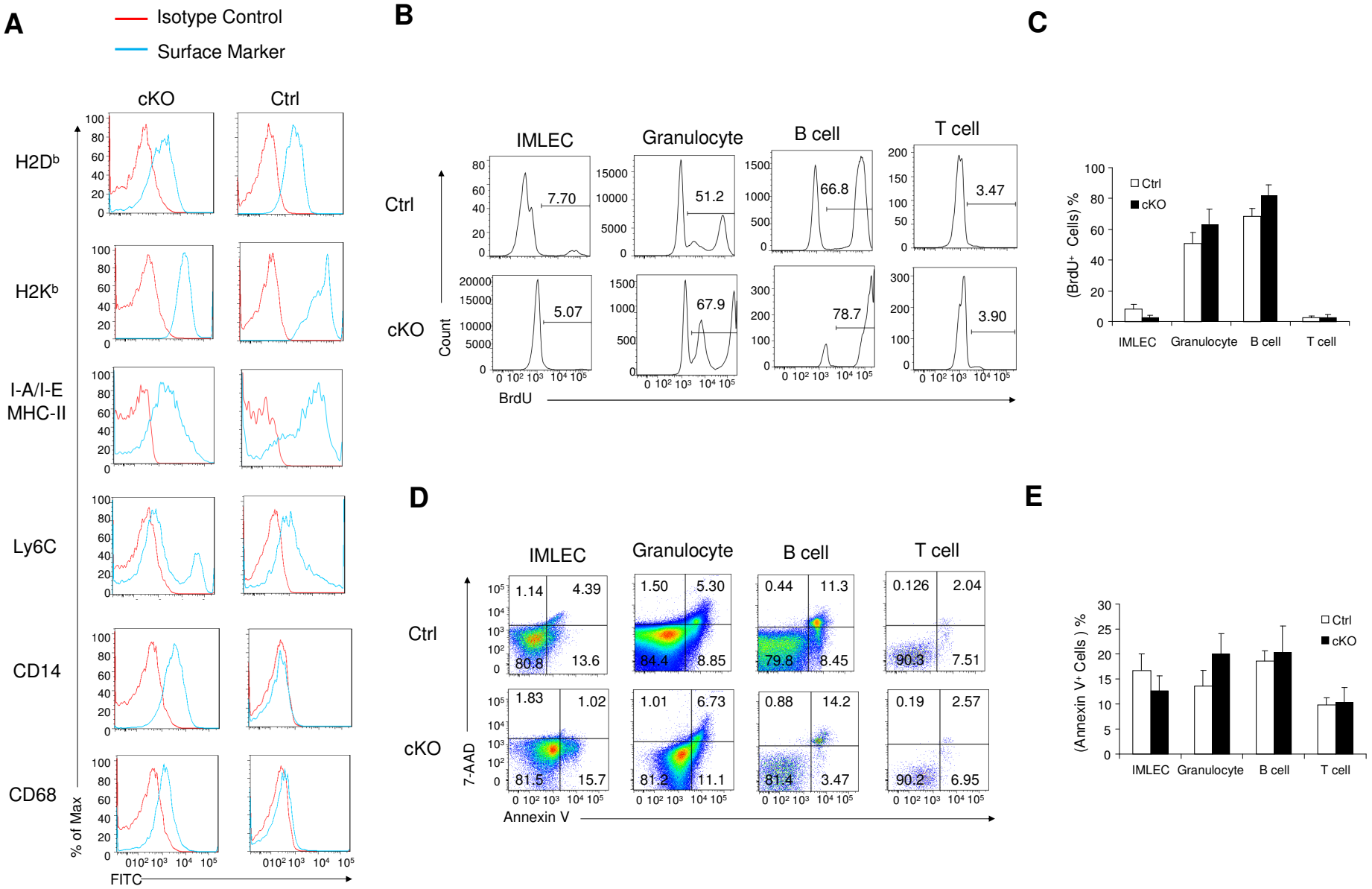

Figure 5

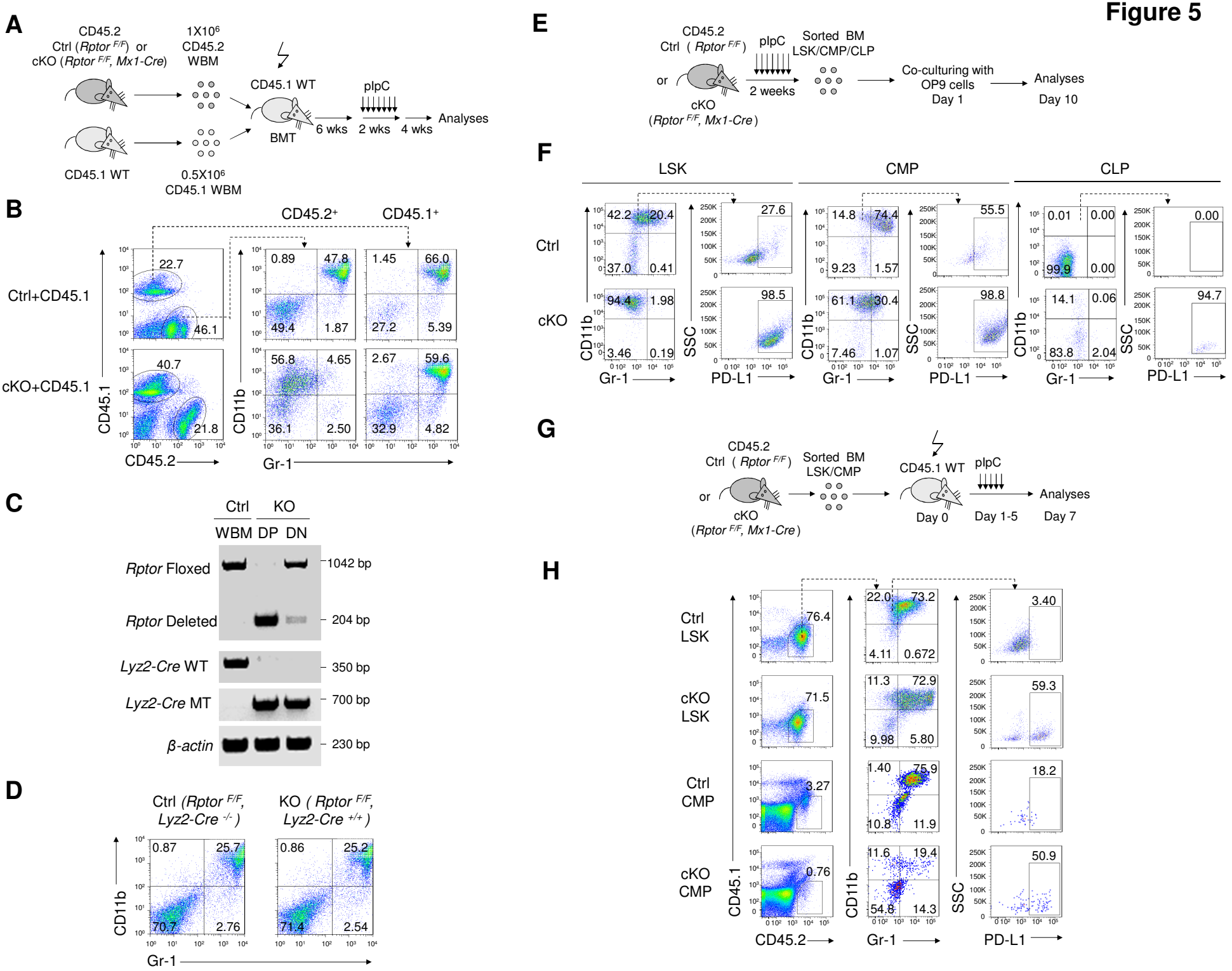
A
CD45.2
Ctrl (Rptor F/F) or
cKO (Rptor F/F, Mx1-Cre)
1X10^6
CD45.2
WBM
CD45.1 WT
0.5X10^6
CD45.1 WBM
CD45.1 WT
BMT
6 wks
pIpC
2 wks
4 wks
Analyses
B
CD45.2+
CD45.1+
Ctrl+CD45.1
cKO+CD45.1
22.7
46.1
40.7
21.8
0.89
47.8
49.4
1.87
1.45
66.0
27.2
5.39
56.8
4.65
36.1
2.50
2.67
59.6
32.9
4.82
CD45.1
CD45.2
CD11b
Gr-1
C
Ctrl
KO
WBM DP DN
Rptor Floxed
Rptor Deleted
Lyz2-Cre WT
Lyz2-Cre MT
β-actin
1042 bp
204 bp
350 bp
700 bp
230 bp
D
Ctrl (Rptor F/F, Lyz2-Cre -/-)
KO (Rptor F/F, Lyz2-Cre +/+)
0.87
25.7
70.7
2.76
0.86
25.2
71.4
2.54
CD11b
Gr-1
E
CD45.2
Ctrl (Rptor F/F)
or
cKO
(Rptor F/F, Mx1-Cre)
pIpC
2 weeks
Sorted BM
LSK/CMP/CLP
Co-culturing with
OP9 cells
Day 1
Analyses
Day 10
F
LSK
CMP
CLP
Ctrl
cKO
42.2
20.4
37.0
0.41
27.6
14.8
74.4
9.23
1.57
55.5
0.01
0.00
99.9
0.00
0.00
94.4
1.98
3.46
0.19
98.5
61.1
30.4
7.46
1.07
98.8
14.1
0.06
83.8
2.04
94.7
CD11b
Gr-1
SSC
PD-L1
G
CD45.2
Ctrl (Rptor F/F)
or
cKO
(Rptor F/F, Mx1-Cre)
Sorted BM
LSK/CMP
CD45.1 WT
Day 0
pIpC
Day 1-5
Analyses
Day 7
H
Ctrl
LSK
cKO
LSK
Ctrl
CMP
cKO
CMP
76.4
22.0
73.2
4.11
0.672
3.40
71.5
11.3
72.9
9.98
5.80
59.3
3.27
1.40
75.9
10.8
11.9
18.2
0.76
11.6
19.4
54.8
14.3
50.9
CD45.1
CD45.2
CD11b
Gr-1
SSC
PD-L1

Figure 6

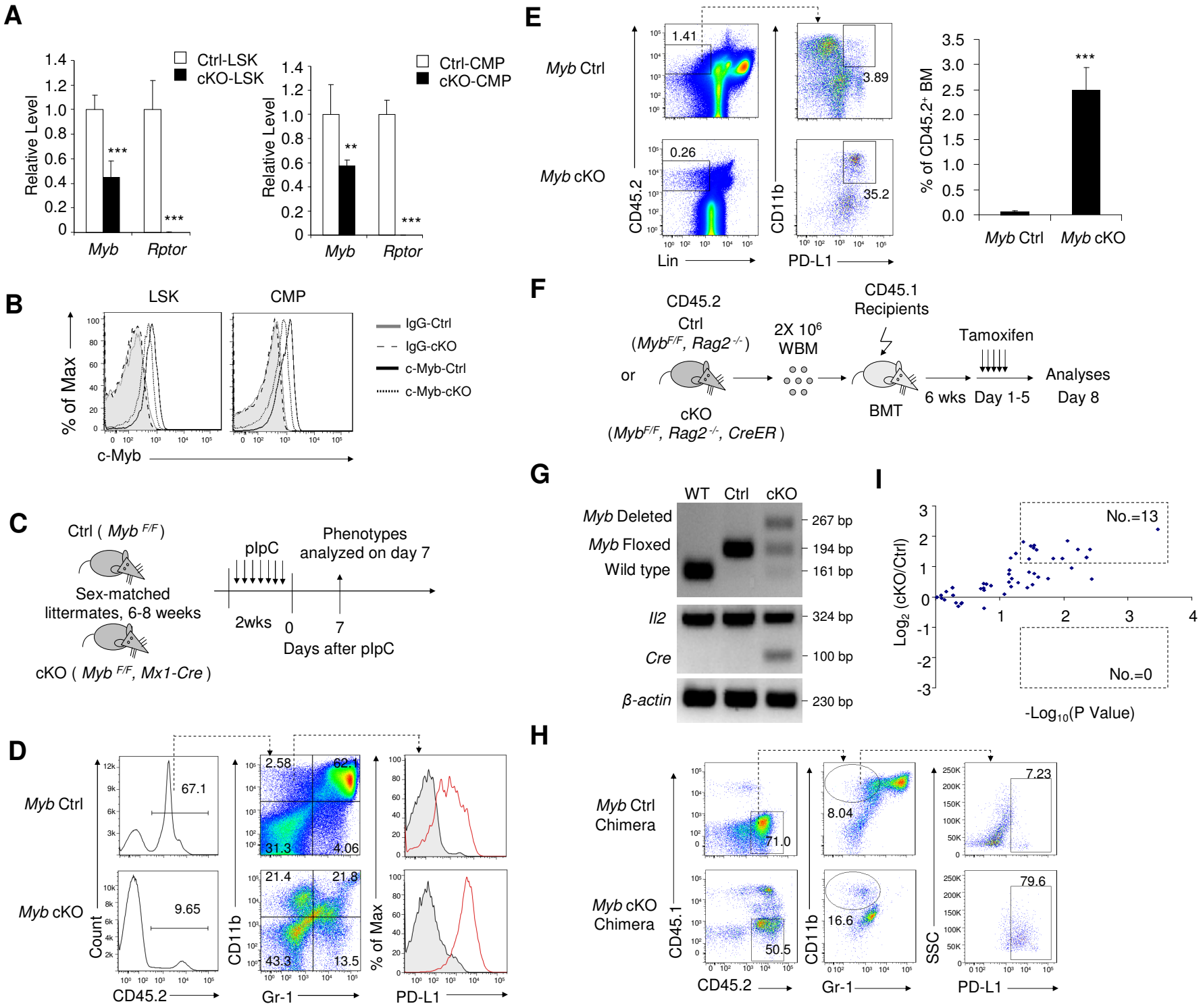
A
Ctrl-LSK
cKO-LSK
Relative Level
Myb
Rptor
Ctrl-CMP
cKO-CMP
B
LSK
CMP
% of Max
c-Myb
IgG-Ctrl
IgG-cKO
c-Myb-Ctrl
c-Myb-cKO
C
Ctrl (Myb F/F)
Sex-matched littermates, 6-8 weeks
cKO (Myb F/F, Mx1-Cre)
pIpC
2wks
0
7
Days after pIpC
Phenotypes analyzed on day 7
D
Myb Ctrl
Myb cKO
Count
CD45.2
CD11b
Gr-1
% of Max
PD-L1
67.1
9.65
2.58
62.1
31.3
4.06
21.4
21.8
43.3
13.5
E
Myb Ctrl
Myb cKO
CD45.2
Lin
CD11b
PD-L1
1.41
3.89
0.26
35.2
% of CD45.2+ BM
F
CD45.2
Ctrl
(MybF/F, Rag2-/-)
or
cKO
(MybF/F, Rag2-/-, CreER)
2X 10^6 WBM
CD45.1 Recipients
BMT
Tamoxifen
6 wks
Day 1-5
Analyses
Day 8
G
WT
Ctrl
cKO
Myb Deleted
Myb Floxed
Wild type
Il2
Cre
β-actin
267 bp
194 bp
161 bp
324 bp
100 bp
230 bp
I
Log2 (cKO/Ctrl)
-Log10(P Value)
No.=13
No.=0
H
Myb Ctrl Chimera
Myb cKO Chimera
CD45.1
CD45.2
CD11b
Gr-1
SSC
PD-L1
71.0
8.04
7.23
50.5
16.6
79.6

Figure 6—figure supplement 1

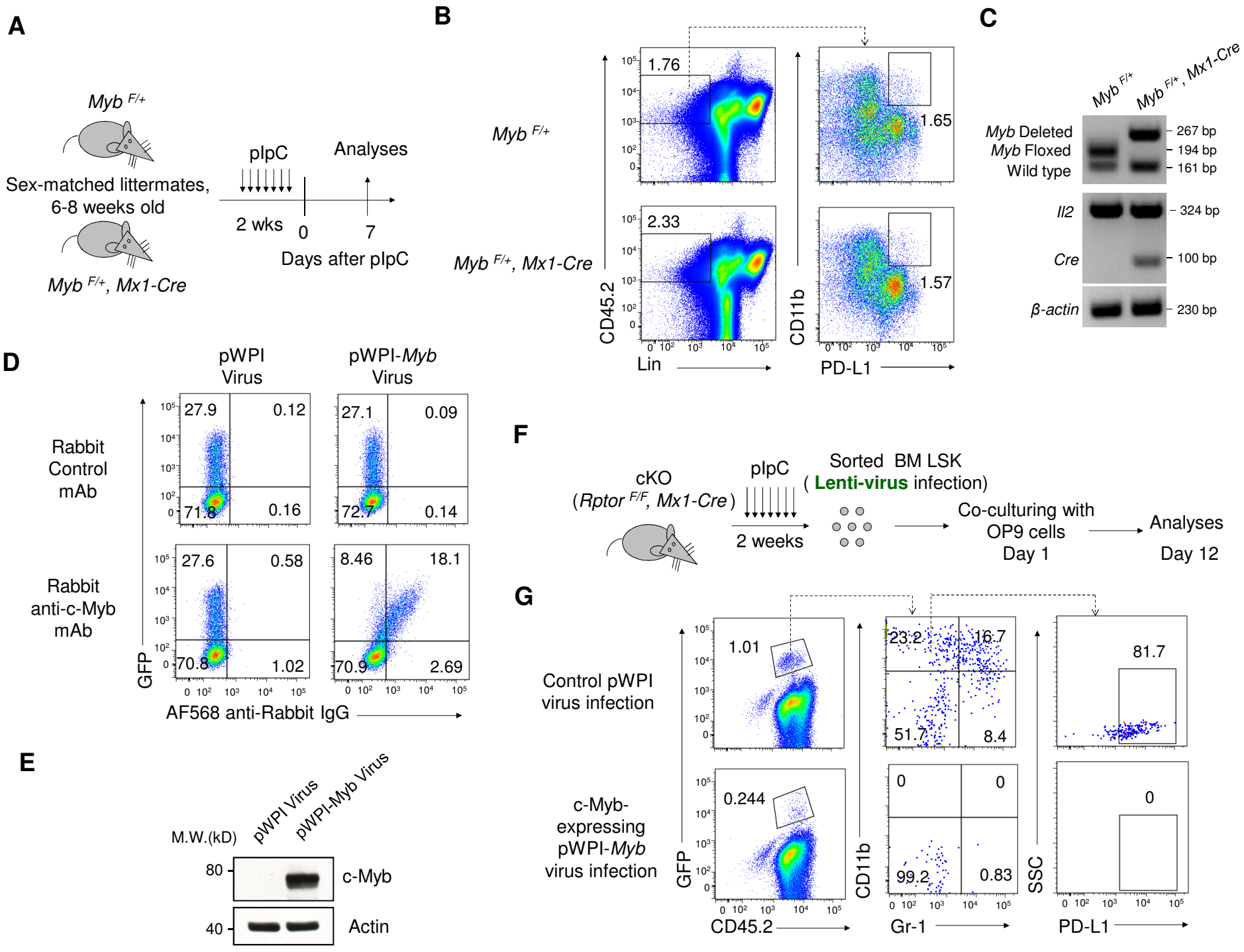

Figure 7

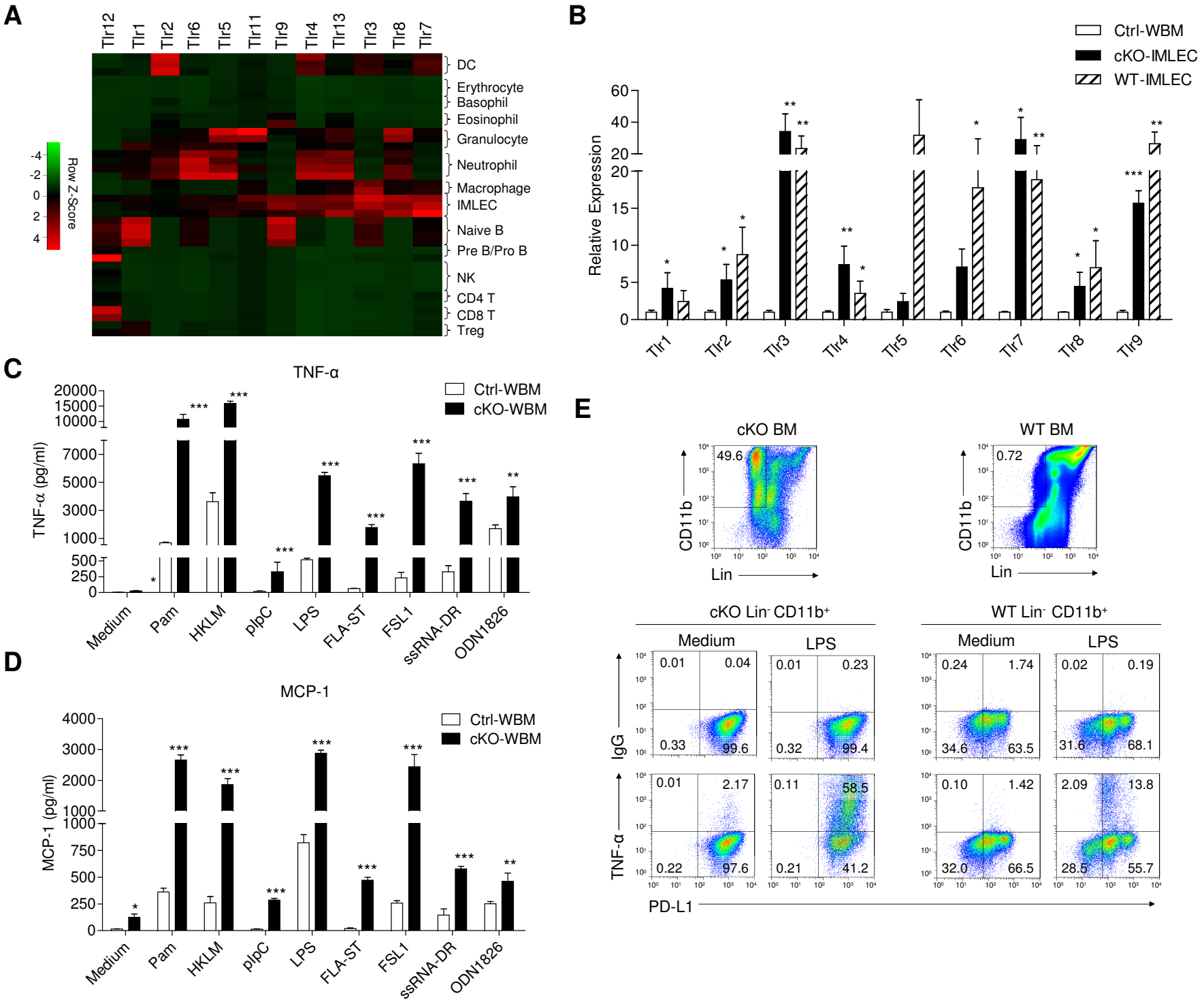
A
Tlr12
Tlr1
Tlr2
Tlr6
Tlr5
Tlr11
Tlr9
Tlr4
Tlr13
Tlr3
Tlr8
Tlr7
DC
Erythrocyte
Basophil
Eosinophil
Granulocyte
Neutrophil
Macrophage
IMLEC
Naive B
Pre B/Pro B
NK
CD4 T
CD8 T
Treg
Row Z-Score
B
Ctrl-WBM
cKO-IMLEC
WT-IMLEC
Relative Expression
C
TNF-α
Ctrl-WBM
cKO-WBM
TNF-α (pg/ml)
Medium
Pam
HKLM
pIpC
LPS
FLA-ST
FSL1
ssRNA-DR
ODN1826
D
MCP-1
MCP-1 (pg/ml)
E
cKO BM
WT BM
CD11b
Lin
cKO Lin⁻ CD11b⁺
WT Lin⁻ CD11b⁺
Medium
LPS
IgG
TNF-α
PD-L1

Figure 7—figure supplement 1

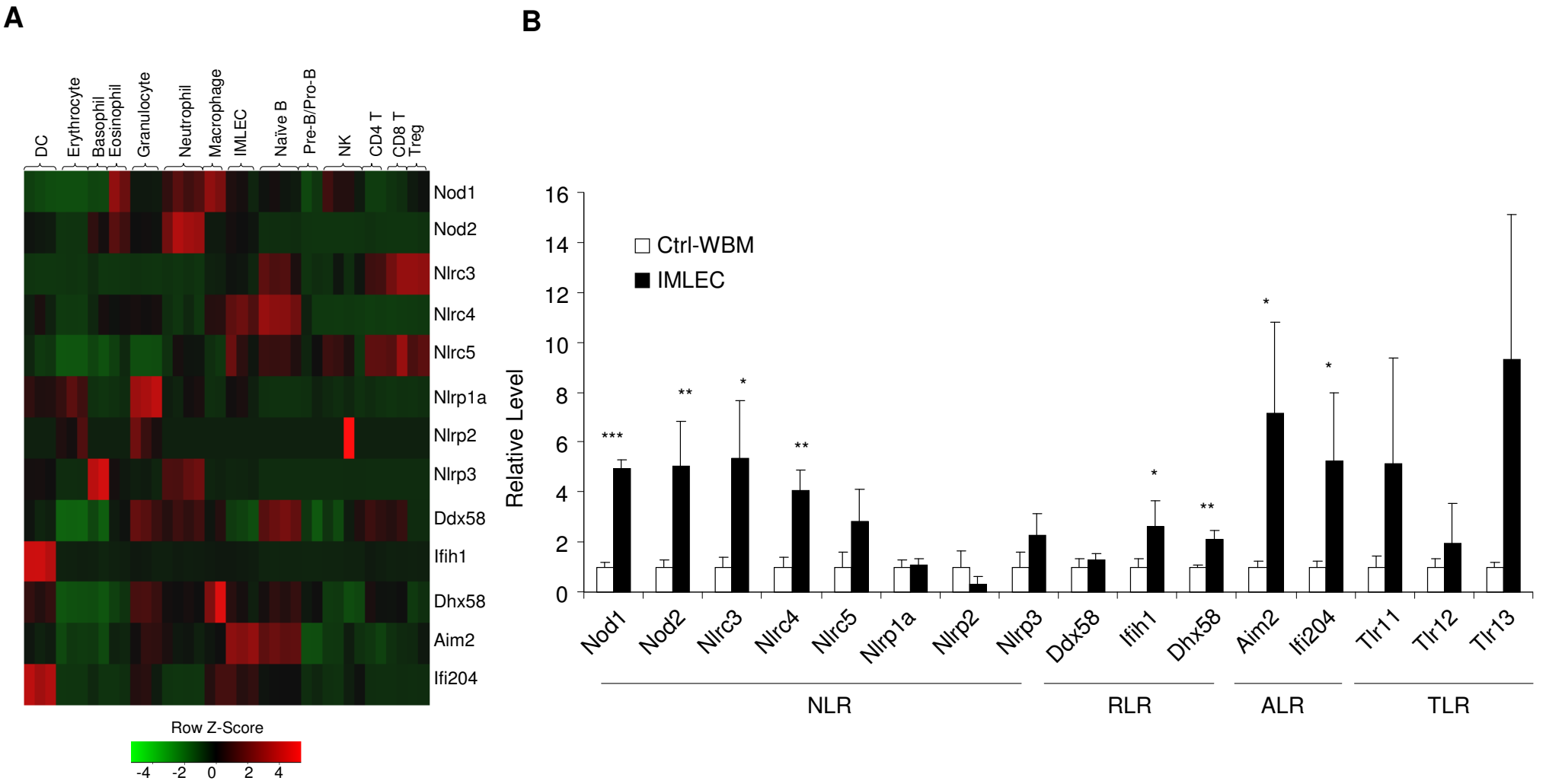

Figure 8

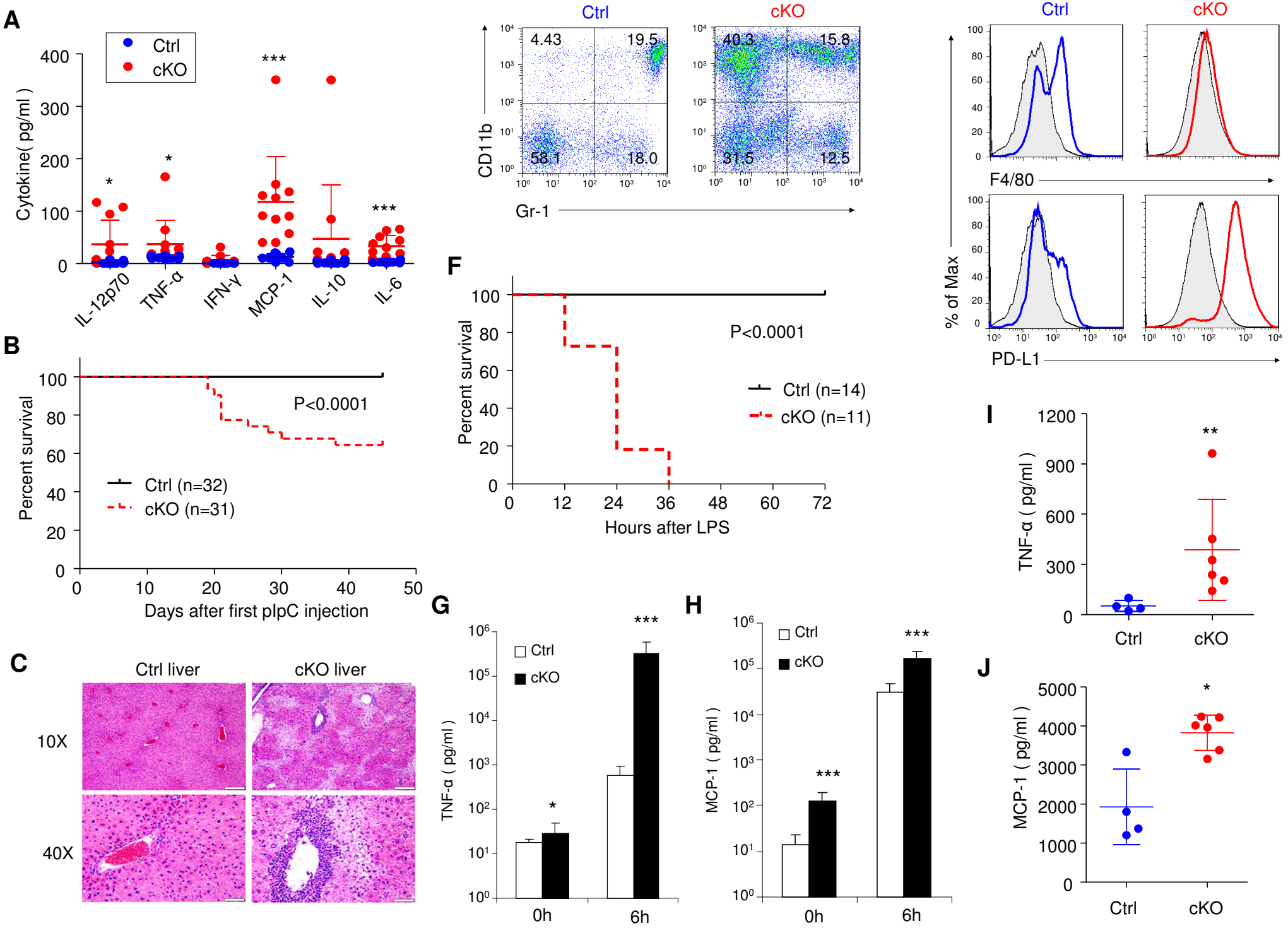
A
Ctrl
cKO
Cytokine(pg/ml)
IL-12p70
TNF-α
IFN-γ
MCP-1
IL-10
IL-6
B
Percent survival
P<0.0001
Ctrl (n=32)
cKO (n=31)
Days after first pIpC injection
C
Ctrl liver
cKO liver
10X
40X
D
Liver Leukocytes
Ctrl
cKO
CD11b
Gr-1
4.43
19.5
58.1
18.0
40.3
15.8
31.5
12.5
E
Liver CD11b+ Gr-1- Cells
F4/80
PD-L1
% of Max
F
Percent survival
P<0.0001
Ctrl (n=14)
cKO (n=11)
Hours after LPS
G
TNF-α (pg/ml)
0h
6h
H
MCP-1 (pg/ml)
I
TNF-α (pg/ml)
J
MCP-1 (pg/ml)

Figure 9

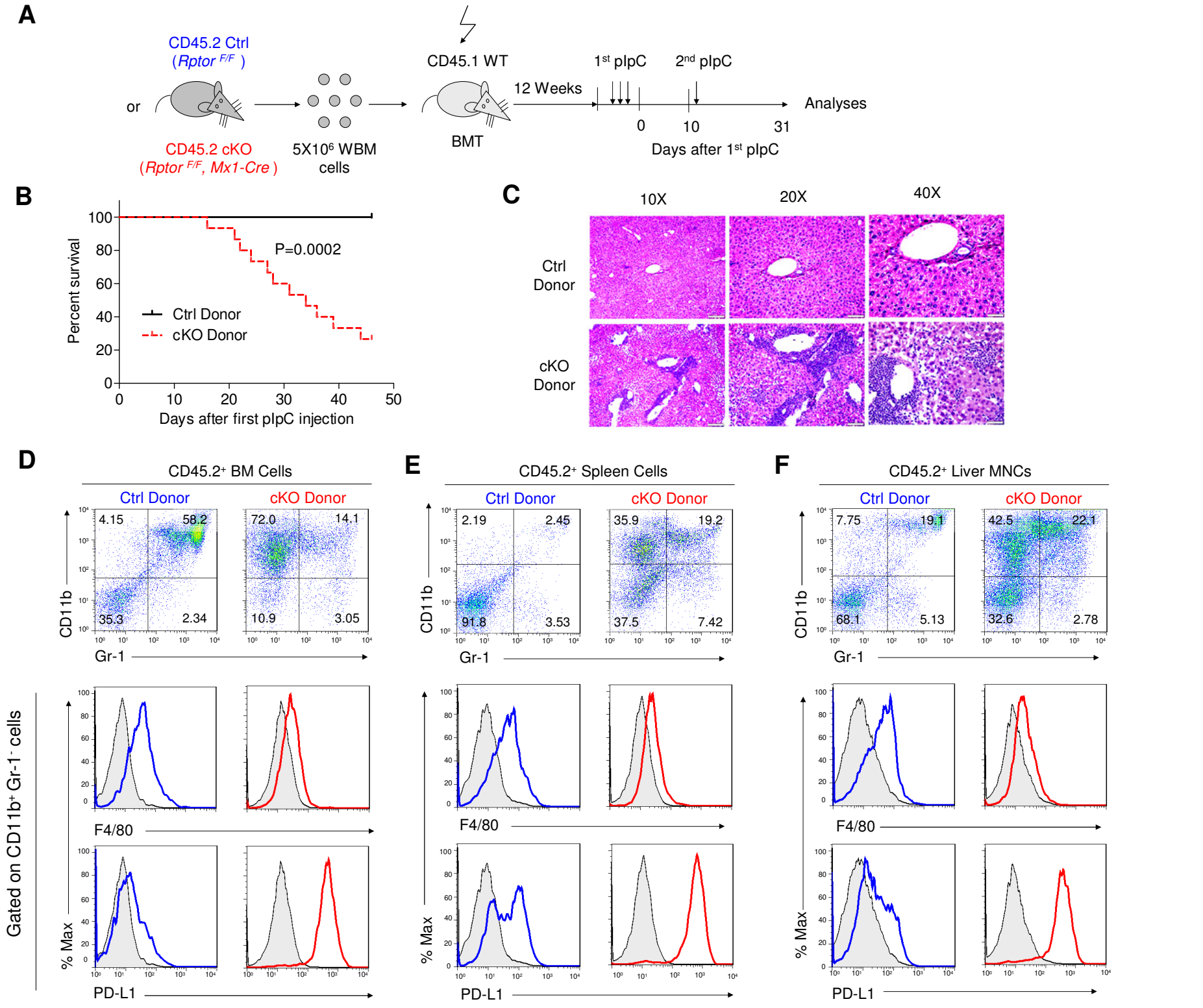
A
CD45.2 Ctrl
(Rptor F/F)
or
CD45.2 cKO
(Rptor F/F, Mx1-Cre)
5X10⁶ WBM
cells
CD45.1 WT
BMT
12 Weeks
1st pIpC
2nd pIpC
0
10
31
Days after 1st pIpC
Analyses
B
Percent survival
P=0.0002
Ctrl Donor
cKO Donor
Days after first pIpC injection
C
10X
20X
40X
Ctrl Donor
cKO Donor
D
CD45.2+ BM Cells
E
CD45.2+ Spleen Cells
F
CD45.2+ Liver MNCs
Ctrl Donor
cKO Donor
CD11b
Gr-1
4.15
58.2
35.3
2.34
72.0
14.1
10.9
3.05
2.19
2.45
91.8
3.53
35.9
19.2
37.5
7.42
7.75
19.1
68.1
5.13
42.5
22.1
32.6
2.78
Gated on CD11b+ Gr-1- cells
F4/80
% Max
PD-L1